

1 Revision 2

2

3 Granitoid magmas preserved as melt inclusions 4 in high-grade metamorphic rocks

5

6 Omar Bartoli^{1*}, Antonio Acosta-Vigil¹, Silvio Ferrero^{2,3}, Bernardo
7 Cesare¹

8

9 ¹*Dipartimento di Geoscienze, Università di Padova, Via Gradenigo 6, 35131 Padova, Italy*

10 ²*Institut für Geowissenschaften, Universität Potsdam, Karl-Liebknecht-Strasse 24/25, D-14476, Golm,*
11 *Germany*

12 ³*Museum für Naturkunde (MfN), Leibniz-Institut für Evolutions- und Biodiversitätsforschung, 10115*
13 *Berlin, Deutschland*

14

15 *corresponding author, omar.bartoli@unipd.it

16

17 **Abstract**

18 This review presents a compositional database of primary anatectic granitoid magmas, entirely based
19 on melt inclusions (MI) in high-grade metamorphic rocks. Although MI are well known to igneous
20 petrologists and have been extensively studied in intrusive and extrusive rocks, MI in crustal rocks that
21 have undergone anatexis (migmatites and granulites) are a novel subject of research. They are generally
22 trapped along the heating path by peritectic phases produced by incongruent melting reactions. Primary
23 MI in high-grade metamorphic rocks are small, commonly 5-10 μm in diameter, and their most
24 common mineral host is peritectic garnet. In most cases inclusions have crystallized into a
25 cryptocrystalline aggregate and contain a granitoid phase assemblage (nanogranitoid inclusions) with
26 quartz, K-feldspar, plagioclase and one or two mica depending on the particular circumstances. After
27 their experimental remelting under high confining pressure, nanogranitoid MI can be analyzed
28 combining several techniques (EMP, LA-ICP-MS, NanoSIMS, Raman). The trapped melt is granitic

29 and metaluminous to peraluminous, and sometimes granodioritic, tonalitic and trondhjemitic in
30 composition, in agreement with the different P-T-a_{H2O} conditions of melting and protolith composition,
31 and overlap the composition of experimental glasses produced at similar conditions. Being trapped
32 along the up-temperature trajectory –as opposed to classic MI in igneous rocks formed during down-
33 temperature magma crystallization– the fundamental information provided by nanogranitoid MI is the
34 pristine composition of the natural primary anatectic melt for the specific rock under investigation. So
35 far ≈600 nanogranitoid MI, coming from several occurrences from different geologic and geodynamic
36 settings and ages, have been characterized. Although the compiled MI database should be expanded to
37 other potential sources of crustal magmas, MI data collected so far can be already used as natural
38 “starting-point” compositions to track the processes involved in formation and evolution of granitoid
39 magmas.

41 **Introduction**

42
43 Granitoid rocks and their extrusive counterparts represent the largest products of magmatic activity on
44 continental crust. In zones of crustal thickening associated with collisional orogens, there are several
45 examples of crystalline basements which have experienced repeated episodes of high-temperature
46 metamorphism, partial melting and extraction of granitoid melts (Sawyer et al., 2011; Brown, 2013).
47 On the other hand, in continental margin arc systems there is much field and geochemical evidence of
48 melting of crustal rocks and hybridization between crustal- and mantle-derived magmas, resulting in
49 the formation of batholiths (Barnes et al., 2002; Annen et al., 2006; Kemp et al., 2007; Gray and
50 Kemp, 2009). Therefore, anatexis of crustal protoliths and formation of anatectic granitoid magmas are
51 key processes for the formation of new crust and its geochemical differentiation (Brown and Rushmer,

52 2006; Hacker et al., 2011; Sawyer et al., 2011). Field geology, experimental petrology, thermodynamic
53 calculations, numerical modeling, whole-rock geochemistry and Hf-O isotopes in zircon represent the
54 major tools for understanding the origin and evolution of anatectic granitoid magmas (see Annen et al.,
55 2006; Brown, 2013; Clemens, 2006; Kemp et al., 2007; Sawyer et al., 2011; White et al., 2011).
56 Despite the vigorous debate on the petrogenesis of granitoid magmas which began more than 60 yr ago
57 (Read, 1948), conflicting views still exist, in particular concerning the melting processes at the source
58 and the differentiation processes which modify granitoid chemistry (Clemens and Watkins, 2001;
59 Clemens and Stevens, 2012, 2015; Brown, 2013; Weinberg and Hasalová, 2015a, b; and discussion
60 therein).

61 Here we present a novel and alternative method to investigate crustal magmas, providing a
62 review of the current research on melt inclusions (MI) in high-grade metamorphic rocks, the source
63 where crustal magmas originate. After discussing the origin of MI by incongruent melting in
64 migmatites, granulites and anatectic enclaves and presenting the data collected mainly by the research
65 group of the authors, along with the adopted experimental and analytical strategies, we highlight how
66 such tiny inclusions of melt can constrain the origin and evolution of granitoid magmas produced by
67 anatexis of crustal rocks.

68

69 **Changing the viewpoint: entrapment of melt inclusions upon heating**

70 MI are small volumes of silicate melt enclosed in minerals (Roedder, 1984). First recognized in the 19th
71 century by Sorby (1858), MI hosted in minerals of igneous rocks have been long studied and widely
72 used in the last forty years (see dataset reported in Kesler et al., 2013), becoming a worldwide-accepted
73 technique to investigate melt evolution in magmatic systems (Clocchiatti, 1975; Roedder, 1979;
74 Sobolev, 1996; Frezzotti, 2001; Schiano, 2003; Bodnar and Student, 2006; Thomas and Davidson,
75 2012; Audétat and Lowenstern, 2014; and references therein). These MI (hereafter “classic MI”) are

76 generally trapped during crystallization of magmas, i.e. along the cooling path where the host crystal is
77 crystallizing *from* the melt which is being entrapped (Fig. 1). MI-bearing phenocrysts in lavas are a
78 typical example of this mode of occurrence. Being trapped along the down-temperature trajectory (Fig.
79 1), such classic MI represent therefore snapshots on the liquid line of descent of silicate liquids (i.e.,
80 they represent variably evolved melts) and, particularly in the case of felsic systems, they have
81 represented a key tool to investigate and understand the genesis of a variety of ore deposits (Audétat
82 and Lowenstern, 2014 and references therein). Even in the case of entrapment by the first liquidus
83 phase (for example olivine in some mantle-derived magmas), classic MI often approximate the
84 composition of the parental melt (i.e., the most primitive melt found in an area) and not that of the
85 primary one (i.e., the melt derived directly by partial melting of the source; see Fig. 1 in Bartoli et al.,
86 2014).

87 In order to represent primary melt compositions, MI should be entrapped in the source region,
88 before magmas undergo segregation and differentiation processes such as mixing and/or mingling with
89 other magma batches, double-diffusive convection, Soret diffusion, cumulus phenomena, fractional
90 crystallization, volatile exsolution and assimilation of residual or exotic material (e.g., Burnham, 1967;
91 DePaolo, 1981; Lesher et al., 1982; Barbarin 1988; Candela, 1997; Weinberg et al., 2001; Stevens et
92 al., 2007; Brown, 2013). Indeed, all these processes produce final products –i.e. most of the extrusive
93 and intrusive rocks we collect in the field– which are markedly different from the original melt
94 produced at the source.

95 The continental crust (i.e. the source region of the anatectic crustal magmas) mostly melts
96 through incongruent melting reactions (Weinberg and Hasalová, 2015a and references therein). Along
97 with magma crystallization, such reactions fulfill the fundamental requirement to form MI, i.e. the
98 growth of a mineral in the presence of a melt phase. Indeed during incongruent melting, both a silicate
99 liquid and a solid phase –the peritectic mineral– are produced contemporaneously along the up-

100 temperature path (Fig. 1). In such a scenario, the peritectic phase can trap droplets of the melt with
101 which it is growing. Shielded by the peritectic host, these MI can provide us with the pristine
102 geochemical signatures (“the starting point” as stated by Sawyer et al., 2011) of magmas formed by
103 crustal anatexis. Although the possibility of trapping droplets of melt during incongruent melting may
104 appear intuitive, MI in high-grade metamorphic rocks have received only little consideration in the past
105 decades. After the first detailed microstructural and microchemical description of MI in regionally
106 metamorphosed granulites of southern India (Cesare et al., 2009), many other occurrences have been
107 reported worldwide in the last six years (e.g. Cesare et al., 2011, 2015; Ferrero et al., 2012, 2014, 2015;
108 Groppo et al., 2012; Mosca et al., 2012; Bartoli et al., 2013a, 2014; Darling, 2103; Kawakami et al.,
109 2013; Barich et al., 2014; Carosi et al., 2015; Massonne, 2014), demonstrating that MI in high-grade
110 metamorphic rocks are more common than expected. More rarely, MI have also been described in
111 enclaves of partially-melted continental crust brought to the Earth’s surface in lavas. This is the case of
112 the anatectic metasedimentary enclaves from the Neogene Volcanic Province (NVP) of southern Spain
113 (Cesare et al., 1997) – also known as “erupted migmatites” (Zeck, 1970). From all the above
114 considerations it is clear that petrologists can utilize a novel tool, i.e. MI trapped by peritectic minerals,
115 to gain previously unavailable information, and to better understand the origins and evolution of crustal
116 magmas.

117

118 **Microstructural characterization of melt inclusions**

119 In most migmatites, granulites and anatectic enclaves investigated so far, MI have been mostly found in
120 garnets of the melt-depleted melanosome portions of the rock (Tab. 1), because this mineral is the most
121 common peritectic phase associated with crustal melting reactions in a wide P – T – X range (see Cesare
122 et al., 2011; Ferrero et al., 2012 and references therein). Other MI-bearing phases are plagioclase and
123 zircon, and less commonly cordierite, andalusite, ilmenite, hercynite and monazite (Tab. 1; Cesare et

124 al., 2015). Crustal enclaves contain abundant MI both in reactants and peritectic phases, e.g.,
125 plagioclase and garnet (Cesare and Maineri, 1999; Cesare et al., 2003; Acosta-Vigil et al., 2007, 2010).
126 Indeed, during melting with some degree of reaction overstepping, some reactant phases in the rock
127 matrix may recrystallize, equilibrate with the melt and trap MI (Cesare et al., 2015).

128 From a microstructural point of view, MI may occur isolated, distributed in zonal arrangements,
129 or in clusters with random distribution within the host mineral (Fig. 2; Ferrero et al., 2012; Barich et
130 al., 2014). These modes of occurrence unequivocally demonstrate the primary nature of MI (Roedder,
131 1979). MI are generally small (<20 μm) and often show negative crystal shape (Fig. 3a-d). Locally,
132 larger MI have been described (up to 150-200 μm , Barich et al., 2014; Ferrero et al., 2015). Variable
133 degrees of crystallization have been observed and MI range from glassy to fully crystallized (Fig. 2e,
134 3a-e). The most common daughter minerals found within crystallized MI are quartz, alkali feldspar,
135 plagioclase, biotite and muscovite (Fig. 3a-c). In MI from near ultrahigh pressure conditions,
136 metastable polymorphs of albite, K-feldspar and quartz have also been identified (Fig. 3b; see also
137 Ferrero et al. 2016). A large number of minerals trapped during inclusion formation has been found
138 within MI, the most common being graphite, zircon, rutile and kyanite. Owing to the very fine grain-
139 size (often <1 μm) and the granitic phase assemblage observed in totally crystallized MI, they have
140 been referred to as “nanogranites” (Cesare et al., 2009). Because recent microchemical investigations
141 have demonstrated the existence of granodiorite, trondhjemite and tonalite compositions (Carosi et al,
142 2015; this study), the totally crystallized polycrystalline MI will be referred, hereafter, to as
143 “nanogranitoid inclusions”. Nanogranitoids can display a diffuse micro- to nano-porosity, which
144 contains liquid H_2O , as evidenced by micro-Raman mapping (Bartoli et al. 2013a). Nanogranitoids may
145 also coexist with primary C-bearing fluid inclusions (Fig. 3f). As both inclusion types are primary, they
146 indicate conditions of fluid-melt immiscibility, thus suggesting COH fluid- present anatexis (Cesare et
147 al., 2007; Ferrero et al., 2011). Preserved glassy MI are abundant in anatectic enclaves owing to the fast

148 cooling (quench) related to the magma uprise and extrusion (Fig. 3d). On the other hand,
149 nanogranitoids and partially crystallized MI are typically found in slowly cooled, regionally
150 metamorphosed migmatite and granulite terranes (Fig. 3a-c). Surprisingly, some preserved glassy MI
151 coexisting with nanogranitoids have been recognized also in migmatitic terranes (Fig. 3e; see also
152 Cesare et al., 2009; Bartoli et al., 2013a,b; Barich et al., 2014). This geological oddity (i.e., the glass
153 preservation in slowly cooled rocks) has been ascribed to either pore size effect (Cesare et al., 2009), or
154 the heterogeneous distribution of nucleation sites (Ferrero et al., 2012), or the high viscosity of the
155 trapped melt (Bartoli et al., 2015).

156

157 **Chemical characterization of melt inclusions**

158 **Re-melting nanogranitoid inclusions**

159 The experimental re-melting of nanogranitoid inclusions is a prerequisite in order to retrieve the
160 original composition (in terms of major and volatile contents) of the trapped melt. Because anatexis
161 takes place in rocks of the middle to lower continental crust, at the bottom of thickened continental
162 crust, and even in continental materials subducted to mantle depths, re-melting experiments of
163 nanogranitoids must be performed under high confining pressure, using a piston-cylinder apparatus, to
164 prevent the inclusion from decrepitating, volatile loss and melt contamination. Indeed, as a
165 consequence of the H₂O loss, crystallized inclusions can be completely re-melted only at temperatures
166 higher than the trapping temperatures –i.e., H₂O loss results in an increased solidus temperature–
167 leading to an inevitable melt-host interaction (see details in Bartoli et al., 2013c). The first attempts to
168 remelt nanogranites using the routine technique in igneous petrology, namely the high-temperature
169 heating stage at ambient pressure (Esposito et al., 2012), produced the decrepitation of the
170 nanogranitoid inclusions, making them poorly suited for a geochemical study (Cesare et al., 2009).

171 The P-T conditions to be used during piston cylinder remelting should be initially established
172 based on phase equilibria modelling or classic thermobarometry, that can provide a fair estimate of the
173 (presumed) P-T conditions of MI entrapment (Bartoli et al., 2013a, c; Ferrero et al., 2015). Conditions
174 of further experiments are then fine-tuned based on the results of the first runs. Despite the time
175 consuming pre- and post-run sample preparation (compared to the heating stage method), and the trial-
176 and-error nature of the experimental approach, this method can successfully re-melt the nanogranitoids
177 under high confining pressure (see Bartoli et al., 2013c; Ferrero et al., 2015).

178

179 **Building up the compositional database**

180 Working with MI in partially melted rocks (i.e. their identification, re-homogenization and chemical
181 characterization) is challenging due to their small diameter, often $<20\ \mu\text{m}$ (Fig. 2, 3). Despite these
182 difficulties, originally glassy and successfully re-melted MI can be analyzed for the concentrations of
183 most elements in the periodic table. Major element contents are routinely measured by electron
184 microprobe (EMP), analyzing secondary standards in the same analytical session to monitor the alkali
185 migration process and eventually calculate correction factors (Ferrero et al., 2012). Indeed, the small
186 size of MI often demands the use of a beam diameter of $\approx 1\ \mu\text{m}$ (Bartoli et al., 2013a), resulting
187 inevitably in Na loss during EMP analysis of hydrous felsic glasses (Morgan and London, 1996,
188 2005a). The Laser Ablation Inductively Coupled-Plasma Mass-Spectrometry (LA-ICP-MS) has been
189 used to measure trace element contents of MI, drilling the glassy MI exposed on the host surface or the
190 nanogranitoid inclusions entirely enclosed in the host. In the latter case, one of the major elements
191 measured by EMP in coexisting glassy or re-melted MI can be used as internal standard for the
192 deconvolution of the mixed signal (Halter et al., 2002). H_2O , which is the most important volatile
193 dissolved in crustal magmas (Burnham, 1975), can be quantified by different methods: deficiency from
194 100% in the EMP analysis (Acosta-Vigil et al., 2007), Raman spectroscopy (Bartoli et al., 2013a;

195 Ferrero et al., 2015) and secondary ion mass spectrometry (SIMS/NanoSIMS: Bartoli et al., 2013c,
196 2014). Using NanoSIMS and Raman spectroscopy, the H₂O concentration of glass can be determined
197 with a high spatial resolution of 1-2 μm . Bartoli et al. (2014) applied different methods to measure H₂O
198 in MI from amphibolite-facies migmatites and observed that, compared to NanoSIMS concentrations,
199 the difference of EMP totals from 100% generally yields slightly higher H₂O contents (up to
200 approximately 15% relative), whereas Raman spectroscopy underestimates H₂O (up to approximately
201 20% relative) when compared to NanoSIMS values. Ferrero et al. (2015) reported lower differences
202 between H₂O values determined by Raman and EMP difference method (approximately 9% relative on
203 the average value).

204 By applying all these techniques, ≈ 600 MI –including re-melted nanogranitoids in migmatites
205 and granulites and glassy MI in anatectic enclaves– have been characterized to date (Fig. 4), leading to
206 the construction of an extensive geochemical database of MI in high-grade metamorphic rocks. In
207 detail, the compositional database consists of ≈ 600 and ≈ 200 major and trace elements analyses,
208 respectively, and ≈ 140 measurements of H₂O by either SIMS, NanoSIMS or Raman. The interested
209 reader may refer to the Supporting Information (Supplementary Tables 1¹ and 2¹) and to Cesare et al.
210 (2015) for tables where all the presented and discussed analyses are reported.

211 The analysed MI come from three continents (Europe, Asia and Africa) and are related to
212 different geologic and geodynamic settings (Tab. 1) such as, i) the late orogenic, low-to-medium P
213 extensional setting represented by the Neogene Volcanic Province of southern Spain, ii) the low-P
214 dynamothermal aureole of Ojén (Betic Cordillera, S Spain), iii) the low- and medium-P collision-
215 related magmatism of the Maghrebian (La Galite, Tunisia) and Himalayan (Kali Gandaki, Nepal)

¹ Deposit item AM-XXX, Supplemental Material. Deposit items are free to all readers and found on the MSA web site, via the specific issue's Table of Contents (go to <http://www.minsocam.org/MSA/AmMin/TOC/>).

216 mountain belts, respectively, iv) the low-to-medium P and ultrahigh-T regional metamorphism of the
217 Kerala Kondalite Belt (India) and v) the near ultrahigh-P metamorphism of the Bohemian Massif
218 (Orlica-Śnieżnik Dome, central Europe). MI have been found in peraluminous metasedimentary
219 rocks and metaluminous metaigneous rocks, and are inferred to have formed at conditions varying from
220 670 to 950 °C and 4 to 27 kbar, from Proterozoic to Quaternary/Pleistocene (Tab. 1). A complete list of
221 published occurrences of MI in migmatites and granulites, along with a description of the host rock and
222 conditions of melting, is reported in Cesare et al. (2015). For the sake of completeness, it should be
223 noted that the research group of the writers has recently found MI also in Proterozoic and Archean
224 rocks from the Americas, as well as from Antarctica and Africa, but their microstructural and
225 microchemical characterization is still in progress.

226

227 **Reliability of the MI as records of melt compositions**

228 During and after entrapment of melt its composition may be modified by several processes, making the
229 MI unrepresentative of the bulk melt in the rock (Roedder, 1984). Many processes such as the
230 crystallization of the host on MI walls, the diffusional exchange of cations between the crystalline
231 phases within nanogranitoids and the host mineral, the nucleation of bubbles by volume contraction
232 and the retrograde fluid infiltration have been widely discussed by Acosta-Vigil et al. (2010, 2012),
233 Bartoli et al. (2013c, 2014) and Cesare et al. (2015). Here, we consider two processes, with which
234 igneous petrologists working with classic MI are more familiar: the boundary layer effect and diffusive
235 H₂O re-equilibration.

236 Boundary layers may develop at the crystal-melt boundary, when the rate of crystal growth is
237 faster than the rate of cation diffusion (Bacon, 1989). This results in a layer immediately adjacent to the
238 growing crystals that is generally depleted in compatible elements and enriched in incompatible
239 elements (Kent, 2008). If these boundary layer melts are trapped as MI, their chemical compositions

240 are obviously not representative of the bulk melt. It should be noted, however, that i) examples of
241 boundary layers have been mainly observed in experimental runs, whereas many studies on natural
242 classic MI do not report compositions affected by boundary layer phenomena –see review papers of
243 Kent (2008) and Audétat and Lowenstern (2014), and ii) experimental boundary layers commonly
244 formed at high degrees of undercooling ($\approx 100\text{--}200\text{ }^{\circ}\text{C}$) around skeletal and dendritic crystals (e.g.
245 Faure and Schiano, 2005; Morgan and London, 2005b). In particular, Faure and Schiano (2005) have
246 demonstrated that the melt trapped in polyhedral crystals is representative of the parental melt, whereas
247 the composition of MI hosted in skeletal or dendritic forsterite crystals lies away from the predicted
248 liquid line of descent. It is important to stress again that MI in high-grade metamorphic rocks are
249 trapped along the heating path in polyhedral peritectic crystals (as opposed to the MI formation during
250 cooling/undercooling in crystallizing magmas). Results from a thorough study of primary MI hosted in
251 garnets of migmatites from the Ojén unit (Betic Cordillera, S Spain) and formed at increasing
252 temperatures (from ≈ 700 to $\approx 820\text{ }^{\circ}\text{C}$), show that MI compositions are mostly controlled by melting
253 conditions, and not by boundary layer systematics. Thus, Fe (compatible with respect to the host
254 garnet) and K (incompatible) are enriched in MI formed at higher temperatures, whereas low-
255 temperature MI have higher H and Na (both incompatible) (Bartoli et al., 2014, 2015). Therefore, the
256 boundary layer effect does not seem to have played an important role in shaping the geochemistry of
257 these trapped melts. Likewise, mass balances show that boundary layer phenomena do not control the
258 differences in major elements compositions among MI hosted in different minerals of anatectic
259 enclaves of SE Spain (Cesare et al., 2015). Regarding the trace element concentrations, MI in several
260 plagioclase and garnet crystals show remarkably similar concentrations in incompatible elements (e.g.
261 Li, Rb, Cs, B, Be, Zn, As, Zr, Th, U), indicating that boundary layer phenomena are negligible for these
262 elements. Conversely, the trace elements compatible or very slightly incompatible in the host (Sr, Ba
263 and Eu for plagioclase, and Y and HREE for garnet) are depleted in the MI due to interaction with the

264 host phase (see Acosta-Vigil et al., 2012). In conclusion, the available data seem to indicate that MI are
265 representative of the bulk melt for the major and incompatible trace elements.

266 Recently, the reliability of olivine-hosted classic MI in preserving the pre-eruptive H₂O
267 contents of degassed lavas has been challenged by experimental studies, which have induced huge H₂O
268 variations in MI within olivine (e.g., from ≈3.8 wt% H₂O to ≈800 ppm; Hauri, 2002; Massare et al.,
269 2002; Portnyagin et al., 2008; Gaetani et al. 2012). On the other hand, Audétat and Lowenstern (2014)
270 have noted that most of the above experiments were done under unrealistic conditions and that many
271 studies on natural MI in olivine demonstrate that the original volatile content of the trapped melt can be
272 preserved after entrapment. Without entering in this “magmatic” dispute, we note that the two
273 contrasting mechanisms of primary MI entrapment (i.e. on the liquidus during crystallization of
274 magmas, and on or close to the solidus during incongruent melting of crustal rocks) along with the
275 contrasting P-T histories may result in different processes affecting the H₂O content of the trapped
276 melts. Compared to crystalline rocks which have experienced prograde anatexis, olivine-hosted MI
277 within magma batches represent the most suitable system for diffusive H₂O re-equilibration. Indeed,
278 during ascent of magmas, important gradients of H₂O concentration and pressure can be continuously
279 formed between the MI and the external magma. On the contrary, in the partially melted crust MI-
280 bearing peritectic phases coexist with discrete fractions of melt scattered in a mostly solid matrix. As
281 discussed by Bartoli et al. (2014), the large differences in physical parameters (e.g. temperature and, in
282 turn, hydrogen diffusivities, pressure and size of MI-bearing crystals) can result in times for the
283 diffusive H₂O re-equilibration which are >10 orders of magnitude greater in migmatitic and granulitic
284 terranes than in the plumbing of magmatic systems.

285 It might be argued that if crustal rocks undergo a long thermal history, reaching temperatures
286 much higher than the trapping temperatures and producing higher amounts of melt, H₂O contents in MI
287 could re-equilibrate with the external drier melt. In this case, three important observations must be

288 taken into account. Firstly, there is much field, microstructural and geochemical evidence indicating
289 that most of the crustal melts generated in the source area have been extracted (Brown, 2013).
290 Secondly, melt accumulation and extraction from anatectic rocks is expected to occur very early after
291 crossing the solidus and to continue during the prograde path, at very low melt fractions (<0.07 ;
292 Rosenberg and Handy, 2005; Jamieson et al., 2011), leaving residual granulites enriched in peritectic
293 minerals (Brown, 2013). Thirdly, very rapid rates of melt extraction have been reported in the
294 literature. For example, Harris et al. (2000) and Villaros et al. (2009) calculated residence times of S-
295 type granites at the source as short as 50 and 500 years, respectively. Therefore, high temperature
296 conditions do not implicitly mean that MI in residual migmatites and granulites experienced diffusive
297 H₂O re-equilibration. The successful re-homogenization of nanogranitoids at temperatures similar to
298 those inferred by phase equilibria calculations or thermobarometry, as reported by Bartoli et al. (2013a,
299 c) and Ferrero et al. (2015), strongly supports the idea that MI can behave as a closed system. Rather,
300 MI compositions could be compromised by fluid infiltration, hydration and retrogression occurring
301 during the subsolidus low-temperature evolution in crystalline basements. However, these processes
302 leave clear microstructural evidence such as the presence of low-temperature minerals within the
303 nanogranitoid inclusions like chlorite (replacing biotite) and pyrite (see Fig. 19 in Cesare et al., 2015).
304 All the above observations strongly suggest that the MI database corresponds to that of primary
305 anatectic melts.

306

307 **Major and trace elements, and H₂O contents**

308 In general, the compiled compositional database for MI in high-grade metamorphic rocks reports
309 compositions rich in SiO₂ (≈ 64 -79 wt%; on a hydrous basis), with variable Al₂O₃ (≈ 10 -18 wt%), Na₂O
310 (≈ 1 -6 wt%) and K₂O contents (≈ 0 -8 wt%) (Fig. 4). Most MI have very low to low-moderate
311 FeO_t+MgO+TiO₂ concentrations (≈ 0.25 -2.5 wt%), whereas a small fraction of the dataset ($\approx 10\%$)

312 show values up to ≈ 4.0 - 5.0 wt%. CaO is low (< 1.5 wt%), except for MI from Kali Gandaki where CaO
313 content can reach values as high as 4 wt% (Fig. 4). H₂O shows extremely variable concentrations (0-12
314 wt%) which are related to different P-T conditions and fluid regimes during crustal melting.

315 Regarding the trace elements, to date the dataset is limited to two case studies from S Spain, i.e.
316 crustal enclaves from El Hoyazo and migmatites from Ojén. Despite the different tectonic settings,
317 anatectic history and host rocks and crystals, the trace elements patterns show remarkably similar
318 characteristics when compared with the composition of the upper continental crust: MI are generally
319 enriched in elements (Cs, Rb, Li, Be and B) partially to totally controlled by muscovite and biotite, and
320 depleted in elements (Ba, Th, REE, Sr, Zr, Hf) hosted by feldspars and accessory phases (zircon and
321 monazite) (Fig. 5; see also Fig. 13 of Acosta-Vigil et al., 2012). Overall, MI from Ojen migmatites are
322 characterized by higher contents of Cs, Rb, B, U, Nb, Zr, Sm, V, Zn, lower contents of Ba and Pb, and
323 variable concentrations of Th, La and Ce with respect to MI in NVP enclaves (Fig. 5). This may reflect
324 differences in bulk host rock compositions and/or mechanisms of anatexis (i.e. different melting
325 reactions, different extent of equilibration between melt and residuum; see Acosta-Vigil et al., 2010,
326 2012).

327

328 **One composition, different types of granitoids**

329 Approximately 20 different classification schemes for granitoid rocks have been proposed in the last 40
330 years (Barbarin, 1999; Frost et al., 2001, and references therein). To describe the composition of crustal
331 magmas trapped in peritectic phases of high-grade metamorphic rocks, we have followed some of the
332 most commonly used classification schemes. Based on their normative compositions and considering
333 the compositional fields of O'Connor (1965), the majority of MI analyzed up to date correspond to
334 granites, whereas nanogranitoids from Kali Gandaki (Nepal) plot in the granodiorite, trondhjemite and
335 tonalite fields (Fig. 6). MI are generally slightly ($ASI=1.0$ - 1.1 ; $ASI = \text{mol. Al}_2\text{O}_3 / (\text{CaO} + \text{Na}_2\text{O} + \text{K}_2\text{O})$)

336 to strongly peraluminous, with ASI up to 1.5 (Fig. 7). However, some proportion of the MI enclosed in
337 orthogneisses of the Bohemian Massif and tonalites of La Galite, are metaluminous or located at the
338 boundary between the metaluminous and peralkaline fields (ASI=0.8-1.0, alkalinity index up to -0.02)
339 (Fig. 7). Chappell and White (1974) proposed the first, modern geochemical scheme for the
340 classification of granitic (s.l.) rocks, and recognized two distinct granitoid types: the S-type
341 (supracrustal type) derived from metasedimentary rocks and the I-type (infracrustal type) inferred to
342 have formed from metaigneous sources (see also Chappell, 1984, 1999; Chappell and White, 1992,
343 2001). Considering their ASI, most analyzed MI correspond to S-type granitoids, with only 8% of the
344 MI plotting in the I-type field (Fig. 7). Remarkably, almost the totality of MI produced from anatexis of
345 metaigneous rocks correspond to I-type granitoid compositions (Fig. 7).

346 Frost et al. (2001) introduced a geochemical classification for granitoid rocks which has
347 achieved wide use (see also Frost and Frost, 2008). Using the compositional parameters suggested by
348 these authors, MI are mostly ferroan granitoids, from alkali-calcic to calc-alkalic, even though some
349 spread can be observed (Fig. 8). MI from Kali Gandaki rocks, instead, depart markedly from the other
350 crustal melts and plot in the calcic field (Fig. 8). As stated by Frost and Frost (2008), calcic
351 compositions are typical of melts produced by fluid-present melting.

352

353 **Insights on the origins and evolution of granitoid magmas**

354 **Melt inclusions and the model (haplo)granite system**

355 The origin of granitoid rocks has been strongly debated in the middle half of the past century by N.L.
356 Bowen and H.H. Read (see Bowen, 1948; Gilluly, 1948; Read 1948). This controversy ended a decade
357 later, when the magmatic origin of granite (s.l.) was definitely demonstrated via experimental petrology
358 by Tuttle and Bowen (1958). These authors showed that melting of a ternary mixture of quartz, albite
359 and orthoclase –i.e. a simple granitic system called haplogranite (Qtz-Ab-Or), starts at relatively low

360 temperatures, typical of the continental crust, provided that the system is H₂O-saturated. After the
361 pioneering work of Tuttle and Bowen (1958), an impressive number of studies have been performed to
362 understand the effect of pressure and H₂O, and to a lesser extent of the other minor components, on the
363 phase relations of the haplogranitic system (Johannes and Holtz, 1996; see below). Also, whole-rock
364 data have been often compared to the eutectic/cotectic compositions of haplogranite system to identify
365 primary compositions of crustal melts (e.g. Olsen and Grant, 1991; Symmes and Ferry, 1995; Slagstad
366 et al., 2005) or to infer the depth of magma-storage (e.g. Blundy and Cashman, 2001; Almev et al.,
367 2012; Gualda and Ghiorso, 2013).

368 Because the haplogranitic system is a relevant reference frame to discuss granite petrogenesis,
369 and because MI in high-grade metamorphic terranes seem to provide the compositions of the primary
370 melts produced by melting of natural crustal rocks, it is important to see how MI data plot in the
371 pseudoternary normative Qtz-Ab-Or diagram. Here, granitoid MI from each locality show some spread
372 and a distinctive composition with respect to each other (Fig. 9a). They are commonly located towards
373 the center of the diagram, often in the Qtz field and above the corresponding cotectic lines at the
374 pressure of melting, between the H₂O-saturated eutectic point and the Qtz-Or join (Fig. 9a).
375 Considering the relatively wide compositional spectrum of the host rocks, it is clear from Figure 9a that
376 the concept of haplogranitic “minimum melt” composition finds little applicability in natural multi-
377 component systems, as even low temperature melts may significantly depart from eutectic
378 compositions. Indeed, natural rocks are more complex than a model system such as the haplogranite,
379 and additional components such as Ca, Ti, Fe and Mg play an important role in modifying the liquidus
380 and solidus phase relationships. For example, Wilke et al. (2015) noted that the effect of An on the
381 phase relationships of the haplogranite system is much more pronounced if small amounts of Fe and Ti
382 (≈ 1 and ≈ 0.2 wt%, respectively) are present.

383 In Figure 9b we have summarized the effects of P, H₂O and other components (e.g. Al and Ca)
384 on the position of the minimum and eutectic points and of the cotectic lines in the ternary system Qtz-
385 Ab-Or, as reported in the literature. MI often cluster above the corresponding cotectic lines, which, in
386 accordance with experimental studies, suggests that excess Al and Ca play an important role in moving
387 the eutectic compositions and the position of cotectic lines towards the Qtz apex (Fig. 9a, b). Most MI
388 show some spread in the Qtz/feldspar ratio compared to their small variation in Ab/Or, forming trends
389 at relatively high angle with the cotectic line (Fig. 9a). This spread of MI data parallel to the Qtz-
390 feldspar direction suggests a control by diffusion in the melt for the major element compositions at the
391 time of MI entrapment (Fig. 9b). Indeed, it has been experimentally shown that the sluggish diffusion
392 of Si and Al versus rapid diffusion of alkalis in granite melts produced by partial melting of quartzo-
393 feldspathic protoliths result in linear trends in the Qtz-Ab-Or diagram (see Fig. 10 in Acosta-Vigil et
394 al., 2006).

395 The decrease of $a_{\text{H}_2\text{O}}$ moves the eutectic point towards the Qtz–Or join without affecting the Qtz
396 content (Fig. 9b). The majority of MI are located between the composition of the H₂O-saturated
397 eutectic and the Qtz–Or side. Although this shift towards higher Or/Ab ratios can be partly related to
398 the presence of Ca in natural systems (Fig. 9b), the collected data support the widespread idea that
399 anatexis and formation of crustal melts generally occur under H₂O-undersaturated conditions (e.g.
400 Thompson, 1990; Clemens and Watkins, 2001). It is important to note, however, that the absence or
401 low proportion of H₂O-saturated melts does not represent a proof for fluid-absent melting, as even
402 H₂O-fluxed melting is generally expected to produce final melts undersaturated in H₂O (Weinberg and
403 Hasalová, 2015b).

404 The reduction of the $a_{\text{H}_2\text{O}}$ during anatexis can be related to two different scenarios: i) melting
405 along a prograde path, in which all the free H₂O present in the rock below the H₂O-saturated solidus is
406 dissolved in the melt at the solidus and melting then continues through fluid-absent reactions; and ii)

407 presence of other components in excess fluids, like the carbonic species CO₂ and CH₄, that reduce the
408 activity of H₂O. A clear example of scenario i) is represented by the Ojén MI. The peraluminous
409 metagreywacke of Ojén underwent prograde anatexis and MI in metatexites represent the first melt
410 produced immediately beyond the fluid-saturated solidus at ≈660-700 °C, ≈4.5-5 kbar (Bartoli et al.,
411 2013c), whereas MI in diatexites reflect the composition of melt formed at higher temperature, under
412 H₂O-undersaturated conditions (≈820 °C; Bartoli et al., 2015). In agreement with this evolution and
413 with the bulk rock composition, MI in diatexites show higher Or/Ab compared to MI in metatexites
414 (Fig. 9a; see also Bartoli, 2012), and the H₂O content of MI decreases from ≈7 to ≈3 wt % with
415 increasing temperature (Bartoli et al., 2015).

416 In scenario ii), the presence in the fluid of carbonic species characterized by low solubility in
417 granitoid melts can result in the phenomenon of immiscibility. As a matter of fact, cordierite, garnet
418 and plagioclase crystals from enclaves of the NVP (SE Spain) preserve spectacular microstructural
419 evidence of immiscible trapping (Fig. 3f), where granitic MI coexist with primary fluid inclusions
420 which are CO₂-dominated (>85 mol%), with minor amounts of N₂ and CH₄, and traces of CO and H₂
421 (see Cesare et al., 2007; Ferrero et al., 2011). Fluid-melt immiscibility is also documented in
422 metaluminous granitoids at La Galite, Tunisia (Ferrero et al., 2014). The origin of CO₂-rich fluids in
423 the deep crust is strongly debated (Santosh and Omori, 2008; Huizenga and Touret, 2012). In the
424 graphite-bearing enclaves from NVP the occurrence of CO₂ has been interpreted as internally generated
425 by Fe³⁺ reduction and graphite oxidation during incongruent melting of biotite (Cesare et al., 2005).
426 Conversely, infiltration of CO₂ from the mantle or from other crustal sources has been postulated for
427 rocks from La Galite (Ferrero et al., 2014).

428 MI from Kerala Khondalite Belt (India) plot very far from haplogranitic minimum melts, close
429 to the Qtz–Or sideline and point to melting temperatures well above minimum or eutectic temperatures,
430 in agreement with the ultra-high temperature (>900 °C) origin of the rocks and the very low H₂O

431 content (≈ 0.7 wt%; Cesare et al., 2009) of the MI. Similar compositions have been obtained by
432 experimental melting of pelitic protoliths at 5-7 kbar, 900-950 °C (Fig. 9a). On the other hand,
433 nanogranitoids from Kali Gandaki (Nepal) are clearly displaced towards the Qtz–Ab sideline and
434 reflect the compositions of crustal melts produced by H₂O-fluxed melting (Carosi et al., 2015). The
435 latter inclusions show the highest H₂O contents (up to 12 wt% by EMP differences) and CaO, and the
436 lowest K₂O (Fig. 4), partly overlapping the composition of experimental glasses produced in the
437 presence of excess H₂O at variable P-T conditions (6-14 kbar, 675-775 °C; Fig. 9a). Indeed, the
438 presence of free H₂O decreases the plagioclase + quartz solidus more strongly than it depresses the
439 stability of micas, producing tonalite/granodiorite/trondhjemite melts (Weinberg and Hasalová, 2015a
440 and references therein). Melt inclusions from the orthogneiss of the Bohemian Massif, re-homogenized
441 at 875 °C and 27 kbar, show the highest content of normative Ab (Fig. 9a) explained by melting at near
442 ultrahigh-P conditions (increasing pressure moves haplogranitic eutectics closer the Ab apex; Fig. 9b).
443 Experimental melts produced at 24-30 kbar, 870-950 °C by melting of different crustal protoliths plot
444 in the same area (Fig. 9a; Ferrero et al., 2015).

445

446 **Characterizing the melting processes at the source**

447 Granitoid MI in high-grade metamorphic rocks are providing more and more robust and consistent
448 information on the chemistry of natural crustal melts (see above). In addition, they represent a new tool
449 to constrain mechanisms (i.e. melting reactions, melting mode, extent of equilibration with the solid
450 residue) and conditions (P-T-a_{H2O}) of formation of crustal magmas, and hence open a new window into
451 the anatectic history of the partially melted continental crust (Fig. 1; Acosta-Vigil et al., 2010).

452 An example of this novel approach is the study of enclaves from El Hoyazo (Neogene Volcanic
453 Province, SE Spain; Acosta-Vigil et al., 2007, 2010, 2012). These rocks represent fragments of
454 continental crust which underwent partial melting and extraction of about 30-60 wt% of granitic melt

455 (Cesare et al., 1997; Cesare, 2008). Here, melt (undevitrified glass owing to rapid cooling of the host
456 dacitic lava) has been chemically investigated both within plagioclase and garnet (see compilation of
457 Fig. 5) and in the rock matrix where it often occurs along foliation planes (i.e. the equivalent of
458 leucosomes in regional migmatites and granulites). Melt inclusions show the highest concentrations of
459 Li, Cs and B, whereas the matrix glass is characterized by higher contents of FRTE (first row transition
460 elements), Y, Zr, Th, REE and higher Rb/Cs and Rb/Li (Fig. 10a; see Acosta-Vigil et al., 2010). The
461 concentrations of Zr and LREE were used to calculate the zircon and monazite saturation temperatures
462 (Watson and Harrison, 1984; Montel, 1993), in order to link MI and potential melt-producing reactions.
463 This approach represents an important advance in granitoid petrology, as the initial temperature of
464 magmas at the source has been long considered to be an inaccessible parameter for allochthonous
465 granites (see Miller et al., 2003). Melt inclusions in plagioclase yield the lowest temperatures (≈ 665 -
466 715 °C), whereas MI in garnet (≈ 685 - 750 °C) and matrix glass (≈ 695 - 800 °C) show higher
467 temperatures (Fig. 10b). Because the analyzed melts seem to be undersaturated to some extent in the
468 accessory phases (Acosta-Vigil et al., 2012), the obtained temperatures have to be considered as
469 minimum estimates (Miller et al., 2003; Acosta-Vigil et al., 2010). In summary, based on the
470 composition of MI within several hosts and matrix glasses, calculated accessory mineral saturation
471 temperatures, and microstructural relationships, it was concluded that the deep crust beneath the
472 Neogene Volcanic Province of SE Spain underwent rapid heating and melting: MI in plagioclase reflect
473 the earliest granitic melts produced by fluid-present to fluid-absent muscovite melting, whereas MI in
474 garnet were produced simultaneously to slightly later via fluid-absent melting of muscovite (Fig. 10c).
475 In contrast, the generation of granitic melts characterized by higher contents of FRTE and REE (the
476 matrix melt) occurred at higher temperatures by biotite dehydration-melting reactions (Fig. 10c). In all
477 cases melt and residual minerals were at, or close to, equilibrium with respect to most trace elements,
478 except for garnet, and some undersaturation in accessory minerals (Acosta-Vigil et al., 2012).

479

480 **The “starting-point” composition**

481 In order to understand which granitoid rocks reflect primary crustal melts and, subsequently, what
482 changes crustal magmas have undergone either near the source region or during their journey towards
483 Earth’s surface, “starting-point” compositions are required (Sawyer et al., 2011). Because leucosomes
484 commonly do not represent primary melts (Sawyer, 2008 and discussion therein), a widespread
485 approach among crustal petrologists is to assume the composition of experimental glasses as
486 representative of crustal melt composition at the source, and to use such composition in mass balance
487 calculations to track the processes involved in magma evolution and crustal differentiation (e.g.,
488 Milord et al., 2001; Solar and Brown, 2001; Barnes et al., 2002; Guernina and Sawyer, 2003; Stevens
489 et al., 2007; Sawyer, 2008; Hacker et al., 2011).

490 The fundamental advance provided by the study of nanogranitoid MI in high-grade
491 metamorphic rocks is that they make accessible the composition of the natural primary anatectic melt
492 for the specific rock under investigation at its specific P-T- X_{H_2O} conditions (Bartoli et al., 2013a;
493 Ferrero et al., 2015; this work). Despite the number of MI analyses is already significant (see above),
494 the compiled MI database should be expanded to cover other potential sources of crustal magmas (e.g.
495 intermediate to mafic protoliths) and a wider spectrum of P-T- a_{H_2O} conditions under which continental
496 crust may melt (i.e. to date the number of MI case studies is still quite low compared to the number of
497 experimental studies). However, the already significant MI dataset collected so far can be already
498 useful to start discussing some of the previously proposed inferences and models regarding crustal
499 melting and the formation and evolution of granitoid magmas. Clearly, in order to make inferences on
500 petrogenetic processes affecting anatectic magmas, and in the absence of specific primary melt
501 compositions from MI for their particular study area, authors should consider using the MI

502 compositions in the published dataset for the conditions (P-T- X_{H_2O} -bulk rock composition) closest to
503 the particular rocks that they are investigating.

504 Figure 11a-d provides the compositional variations of MI in terms of mol% of $Fe_{Tot}+Mg+Ti$,
505 $Na+Ca$, K and $Si+Al$. The major crystalline phases are reported along with MI data. These types of
506 diagrams have been previously used to model crustal reworking by anatexis (see Solar and Brown,
507 2001; Barnes et al., 2002; Korhonen et al. 2010; Farina et al., 2015; Yakymchuk et al., 2015). Host
508 rock compositions form different clusters according to their nature (for example, metapelites show the
509 highest $Fe_{Tot}+Mg+Ti$ values whereas metagreywackes are enriched in Si and K); MI plot away from
510 the $Fe_{Tot}+Mg+Ti$ apex, into the bottom half of the diagrams at variable $(Na+Ca)/K$ and
511 $(Na+Ca)/(Si+Al)$ ratios, providing a slightly variable though distinctive melt composition (Fig. 11a-d).
512 This is in agreement with the fact that the composition of the source and conditions of anatexis play a
513 major control on melt chemistry.

514 The Himalayan Leucogranites (HL) are commonly considered to represent nearly pure melts
515 produced by low-temperature (≈ 700 °C) melting of metapelites and metagreywackes (Le Fort et al.,
516 1987). As a matter of fact, most HL overlap with the low-temperature MI (i.e those hosted in garnet
517 from the Ronda metatexites and in garnet and plagioclase of NVP enclaves), supporting their primary
518 nature (Fig. 12e, f). Some HL compositions, however, do not resemble MI compositions and plot in the
519 proximity of the lower portion of the field occupied by most MI data (Fig. 11e, f). It is important to
520 note that the difference in mafic components (Fe, Mg and Ti) between HL and MI cannot be related to
521 contamination of MI by the host phase during analysis, as MI hosted in Fe-, Mg- and Ti-free hosts such
522 as plagioclase show similar and sometimes higher $Fe+Mg+Ti$ contents with respect to MI hosted in
523 garnet (Fig. 11b, d). On one hand, the observed discrepancy can be related to an incomplete MI dataset
524 (i.e. incomplete sampling of MI in high-grade metamorphic rocks). On the other hand, it could indicate
525 a non-primary nature of some HL. For instance, Scailett et al. (1990) stated that some geochemical

526 features of Gangotri leucogranites (for which compositions sometimes depart from those of MI; Fig.
527 11e) can be explained by fractionation of the early crystallizing phases. Their compositions often
528 depart from the compositions of primary HL in the opposite direction of the Bt and Ms fields (Fig. 11e,
529 f). As a matter of fact, some Gangotri leucogranites have lower Co, V and B contents than MI in Ronda
530 metatexites and lower Li content than MI in garnet of NVP, in agreement with a mica fractionation
531 process. It should be noted that petrographic and experimental evidence indicate that biotite was likely
532 the first mineral to crystallize in many HL (Scaillet et al., 1995). Therefore, the available MI data seem
533 to support a primary nature for the majority of HL, even though fractional crystallization processes
534 might have occurred locally, in agreement with results from previous studies (i.e. Le Fort et al., 1987;
535 Scaillet et al., 1990). It is important to note that MI from Kali Gandaki (Nepal) represent Ca-rich melts
536 produced during Eocene prograde metamorphism (Carosi et al., 2015; Iaccarino et al., 2015) and,
537 therefore, they are not related to the Miocene HL formed during exhumation stage (Harris and Massey,
538 1994).

539 The Layos Granite (Toledo Complex, central Spain) represents a S-type, strongly peraluminous
540 Crd-bearing granitoid suite, varying from quartz-rich tonalite to melamonzogranites and formed at
541 about 800-850 °C by biotite melting of metapelites (Barbero and Villaseca, 1992). Most of these rocks
542 plot away from MI datasets, towards the $Fe_{Tot}+Mg+Ti$ apex (Fig. 11e, f). The authors explained the
543 observed compositional variability of the suite by a “restite unmixing” model (Barbero and Villaseca,
544 1992). This model was proposed by Chappell et al. (1987) to explain the geochemical variability of
545 granitoid rocks and states that the majority of granites represent mixtures between a low-T melt and the
546 restite, i.e. solid materials that were residual from the source. Therefore, granites were thought to image
547 their source in a simple way: compositional variations observed within granitoid suites reflect varying
548 degrees of restite unmixing with a minimum or near-minimum temperature (haplogranitic) melt
549 (Chappell et al., 1987). However, this model has received several criticisms from the geochemical,

550 petrographic and physical point of view (see Wall et al., 1987; Clemens and Mawer, 1992; Clemens,
551 2003; Vernon, 2010; Clemens and Stevens, 2012 for additional details). The fact that the composition
552 of the primary melt produced in the source may differ markedly from that of minimum melt, as clearly
553 demonstrated by MI study (see discussion above), demonstrates that the assumption that the melt
554 component has an eutectic composition is not applicable in natural systems. Recently, Stevens et al.
555 (2007) and Clemens and Stevens (2012) proposed a revised version of the restite unmixing model,
556 called “peritectic assemblage entrainment” or “selective peritectic phase entrainment”. Following this
557 model, the more mafic granitoid rocks result from the entrainment of the solid peritectic products of the
558 melting reaction to the melt (although how this would occur is not fully explained), rather than from the
559 entrainment of a proportion of the total solid mineral assemblage remaining after the melting reaction.
560 Regarding the Layos Granite, only one data point plots in the MI field (overlapping the composition of
561 MI trapped in Crd from metapelites and formed at $\approx 850^\circ\text{C}$; Fig. 11e, f) and, in turn, seems to reflect a
562 primary origin. The rest of data plots between this primary melt composition and the $\text{Fe}_{\text{Tot}}+\text{Mg}+\text{Ti}$ apex
563 and does not form a trend towards the $(\text{Si}+\text{Al})/10$ apex. Similarly, in the $(\text{Fe}_{\text{Tot}}+\text{Mg}+\text{Ti})-(\text{Si})-(\text{Al})$
564 diagram (not shown), Layos granites do not show compositional trends towards the Si and Al apexes.
565 According to the model proposed by Stevens et al. (2007), this chemical signature can be explained by
566 differential entrainment of peritectic cordierite (up to 30% of Crd has been documented in these rocks),
567 without the involvement of residual Qtz and Als, i.e. the restite unmixing model does not seem to be
568 applicable in this specific case.

569 The Malani rhyolites (western India) are considered to be the product of high-T crustal anatexis
570 (Maheshwari et al., 1996), and the fact that the majority of lava compositions match those of MI
571 supports their primary origin (Fig. 11c). Strongly peraluminous, K-rich Malani rhyolites resemble the
572 glassy MI from Kherala Khondalite Belt, in agreement with the inference that the rhyolites were likely
573 produced by melting of metapelites at temperatures $\geq 850^\circ\text{C}$ (Maheshwari et al., 1996). At the same

574 time, the comparison with MI would suggest a more complex scenario for the genesis of these anatectic
575 lavas. Malani rhyolites have variable (Na+Ca)/K ratio and some lava compositions overlap the
576 compositions of MI found in NVP metapelitic enclaves, Ronda metatexites and La Galite granodiorite
577 and formed at variable temperatures ($\approx 700\text{-}820\text{ }^{\circ}\text{C}$) (Fig. 11c). These lavas range from peraluminous,
578 through metaluminous to peralkaline. Notably, almost the totality of metaluminous/peralkaline lavas
579 approach the metaluminous/peralkaline compositions of MI from La Galite granodiorite. The observed
580 compositional variability can reflect the presence of distinct magma batches in the Malani rhyolite
581 complex, formed and extracted during prograde heating of a compositionally heterogeneous crustal
582 source. In this sense, other work has verified the occurrence of a heterogeneous crystalline basement
583 (composed of both granodiorites, orthogneisses and metasedimentary rocks) beneath Malani rhyolites
584 (Pandit et al., 1999; Sharma, 2004). Instead a single composition seems to reflect the entrainment of
585 mafic minerals (Fig. 11c).

586 In Figure 12 we have compared the composition of MI with a dataset of ≈ 520 experimental glasses
587 reported in literature and produced at variable P-T- $a_{\text{H}_2\text{O}}$ conditions and using different starting
588 materials, i.e., metasedimentary and felsic (meta)granitoid protoliths. Remarkably, MI and glasses from
589 experiments seem to be characterized by similar compositions and compositional ranges, even though
590 experimental melts may show higher $\text{Fe}_{\text{Tot}}+\text{Mg}+\text{Ti}$ values than MI (Fig. 12). Koester et al. (2002)
591 reported glasses, produced at 700°C and 5-15 kbar, characterized by anomalously high FeO, TiO_2 and
592 MgO contents (e.g., $\text{FeO} \approx 9.5\text{ wt}\%$; see red dots in Fig. 12), in contrast with their low-temperature
593 origin. The authors argued that the lack of chemical equilibrium was responsible for the heterogeneous
594 chemical compositions of melt observed in near-solidus experiments (Koester et al., 2002; see also
595 Gardien et al., 1995). Indeed, as any other petrologic tool, partial melting experiments may suffer from
596 potential pitfalls, in particular: impossibility of bulk compositional changes (in experiments there is no
597 H_2O and melt loss), slow kinetics of reactions, loss of iron from silicate phases to experimental

598 capsules, lack of equilibration, overstepping of melting reactions and difficulty of obtaining reliable
599 glass analyses in near-solidus experiments (Ratajeski and Sisson, 1999; Gardien et al., 2000; White et
600 al., 2011; Webb et al., 2015). Nonetheless, when the low-temperature (≤ 720 °C) experiments are
601 considered, with the exception of the analyses reported in Koester et al. (2002), the produced melts
602 show low and variable $Fe_{Tot}+Mg+Ti$ contents, overlapping the compositions of low-temperature MI
603 (Fig. 12).

604 From all the above considerations, it is clear that MI are an useful tool with which to discuss the
605 petrogenesis of granitoid rocks, and can complement experimental glasses to constrain differentiation
606 processes occurring in anatectic magmas. Researchers working on petrogenesis of crustal granitoids
607 can now look for and study MI in migmatites and granulites considered to be the source region of the
608 studied magmas, or in peritectic garnet entrained in the granitoid rocks in order to fix the real primary
609 composition for their specific case study. In particular, as the number of experimental studies presently
610 reporting trace element composition of melt is limited, MI are an important contribution that provides
611 the trace element compositions of natural anatectic melts.

612

613

Implications

614 Nanogranitoid melt inclusions in high-grade metamorphic rocks are a novel subject of research and are
615 becoming a matter of considerable scientific interest, as they allow the analysis *in situ* of the natural
616 primary melts produced by crustal melting. The size of nanogranitoid MI (commonly 10 μm in
617 diameter) and of daughter minerals crystallized in them (often ≤ 1 μm) pose analytical challenges, and
618 the accurate re-homogenization and compositional characterization of these small data repositories is
619 far from being routine. However, we have shown here that, albeit slowed down by many experimental
620 and analytical difficulties, the study of these MI opens new horizons for metamorphic and igneous
621 petrology. Technological improvement in the coming years will make the study of MI easier, and we

622 believe that their chemical characterization, in particular of volatiles, trace elements and radiogenic
623 isotopes, will provide exciting new results in many topics, such as granitoid petrogenesis, UHT and
624 UHP metamorphism, secular variations of felsic magmatism, volatile recycling, crust formation and
625 silicate Earth differentiation.

626 **Acknowledgements**

627 Many thanks to Edward Sawyer and Chris Yakymchuck for their reviews of the manuscript and to Cal
628 Barnes for the editorial handling. This research benefitted from funding from the Italian Ministry of
629 Education, University, Research (grant SIR RBSI14Y7PF to OB and grant PRIN 2010TT22SC to BC),
630 from Padova University (Progetti per Giovani Studiosi 2013 to OB, Progetto di Ateneo
631 CPDA107188/10 to BC and Piscopia — Marie Curie Fellowship GA No. 600376 to AAV), from the
632 Ministerio de Ciencia e Innovación of Spain (grant CGL2007-62992 to AAV), and from the Alexander
633 von Humboldt Foundation, the German Federal Ministry for Education and Research and the Deutsche
634 Forschungsgemeinschaft (Project FE 1527/2-1 to SF). The research leading to these results has
635 received funding from the European Commission, Seventh Framework Programme, under Grant
636 Agreement n° 600376.

637

638 **References**

639 Acosta-Vigil, A., London, D., and Morgan, G.B. VI (2006) Experiments on the kinetics of partial
640 melting of a leucogranite at 200 MPa H₂O and 690-800 °C: compositional variability of melts during
641 the onset of H₂O -saturated crustal anatexis. *Contributions to Mineralogy and Petrology*, 151, 539–
642 557.

643 Acosta-Vigil, A., Cesare, B., London, D., and Morgan, G.B. VI (2007) Microstructures and
644 composition of melt inclusions in a crustal anatectic environment, represented by metapelitic

- 645 enclaves within El Hoyazo dacites, SE Spain. *Chemical Geology*, 237, 450–465.
- 646 Acosta-Vigil, A., Buick, I., Hermann, J., Cesare, B., Rubatto, D., London, D., and Morgan VI, G.B.,
647 (2010) Mechanisms of crustal anatexis: a geochemical study of partially melted metapelitic enclaves
648 and host dacite, SE Spain. *Journal of Petrology*, 51, 785–821.
- 649 Acosta-Vigil, A., Buick, I., Cesare, B., London, D., and Morgan, G.B. V.I. (2012) The extent of
650 equilibration between melt and residuum during regional anatexis and its implications for
651 differentiation of the continental crust: a study of partially melted metapelitic enclaves. *Journal of*
652 *Petrology*, 53, 1319–1356.
- 653 Almeev, R.R., Bolte, T., Nash, B.P., Holtz, F., Erdmann, and M., Cathey, H. (2012) High-temperature,
654 low-H₂O silicic magmas of the Yellowstone Hotspot: an experimental study of rhyolite from the
655 Bruneau–Jarbidge eruptive center, central Snake River Plain, USA.
- 656 Annen, C., Blundy, J.D., and Sparks, R.S.J. (2006) The genesis of intermediate and silicic magmas in
657 deep crustal hot zones. *Journal of Petrology*, 47, 505–539.
- 658 Audetat, A., and Lowenstern, J.B. (2014) Mel inclusions. In: H.D. Holland and K.K. Turekian, Eds.,
659 *Treatise on Geochemistry (Second Edition)*, p. 143–173. Elsevier, Oxford.
- 660 Auzanneau, E., Vielzeuf, D., and Schmidt, M.W., (2006) Experimental evidence of decompression
661 melting during exhumation of subducted continental crust. *Contributions to Mineralogy and*
662 *Petrology*, 152, 125–148.
- 663 Bacon, C.R. (1989) Crystallization of accessory phases in magmas by local saturation adjacent to
664 phenocrysts. *Geochimica et Cosmochimica Acta*, 53, 1055–1066.
- 665 Barbarin, B. (1988) Field evidence for successive mixing and mingling between the Piolard Diorite and
666 the Saint-Julien-la-Vêtre Monzogranite (Nord–Forez, Massif Cen- tral, France). *Canadian Journal of*
667 *Earth Sciences*, 25, 49–59.

- 668 Barbarin, B. (1999) A review of the relationships between granitoid types, their origins and their
669 geodynamic environments. *Lithos*, 46, 605–626.
- 670 Barbero, L., and Villaseca, C., (1992) The Layos granite, Hercynian complex of Toledo (Spain): an
671 example of parautochthonous restite-rich granite in a granulitic area. *Transaction of the Royal*
672 *Society of Edinburgh Earth Sciences*, 83, 127–138.
- 673 Barich, A., Acosta-Vigil, A., Garrido, C.J., Cesare, B., Tajcmanová, L., and Bartoli, O. (2014)
674 Microstructures and petrology of melt inclusions in the anatectic sequence of Jubrique (Betic
675 Cordillera, S Spain): Implications for crustal anatexis. *Lithos* 206–207, 303–320.
- 676 Barnes, C.G., Yoshinobu, A.S., Prestvik, T., Nordgulen, Ø., Karlsson, H., and Sundvoll, B. (2002)
677 Mafic magma itraplating: anatexis and hybridization in arc crust, Bindal Batholith, Norway. *Journal*
678 *of Petrology*, 43, 2171–2190.
- 679 Bartoli, O. (2012) When the continental crust melts: a combined study of melt inclusions and classical
680 petrology on the Ronda migmatites., 128 p. Ph.D. thesis, University of Parma, Italy. □
- 681 Bartoli, O., Cesare, B., Poli, S., Bodnar, R.J., Acosta-Vigil, A., Frezzotti, M.L., and Meli, S. (2013a)
682 Recovering the composition of melt and the fluid regime at the onset of crustal anatexis and S-type
683 granite formation. *Geology*, 41, 115–118.
- 684 Bartoli, O., Tajcmanová, L., Cesare, B. and Acosta-Vigil, A., (2013b) Phase equilibria constraints on
685 melting of stromatic migmatites from Ronda (S. Spain): insights on the formation of peritectic
686 garnet. *Journal of Metamorphic Geology*, 31, 775–789.
- 687 Bartoli, O., Cesare, B., Poli, S., Acosta-Vigil, A., Esposito, R., Turina, A., Bodnar, R.J., Angel, R.J.,
688 and Hunter, J. (2013c) Nanogranite inclusions in migmatitic garnet: behavior during piston cylinder
689 re-melting experiments. *Geofluids*, 13, 405–420. □
- 690 Bartoli, O., Cesare, B., Remusat, L., Acosta-Vigil, A., and Poli, S. (2014) The H₂O content of granite
691 embryos. *Earth and Planetary Science Letters*, 395, 281–290. □

- 692 Bartoli, O., Acosta-Vigil, A., and Cesare, B. (2015) High-temperature metamorphism and crustal
693 melting: working with melt inclusions. *Periodico di Mineralogia*, *Periodico di Mineralogia* 84,
694 <http://dx.doi.org/10.2451/2015PM00xx>.
- 695 Becker, A., Holtz, F., and Johannes, W. (1998) Liquidus temperatures and phase compositions in the
696 system Qz-Ab-Or at 5 kbar and very low water activities. *Contributions to Mineralogy and*
697 *Petrology*, 130, 213–24.
- 698 Blundy, J., and Cashman, K. (2001) Ascent-driven crystallization of dacite magmas at Mount St
699 Helens, 1980–1986. *Contributions to Mineralogy and Petrology*, 140, 631–650.
- 700 Bodnar, R.J., and Student, J.J. (2006) Melt inclusions in plutonic rocks: Petrography and
701 microthermometry. In: J.D. Webster, Ed., *Melt inclusions in plutonic rocks*, p. 1–26. Mineralogical
702 Association of Canada Short Course 36.
- 703 Bowen, N.L. (1948) The granite problem and the method of multiple prejudices. In: J. Gilluly, Ed.,
704 *Origin of Granite*, p. 79–90. Geological Society of America Memoir 28.
- 705 Brearley, A.J., and Rubie, D.C. (1990) Effects of H₂O on the disequilibrium breakdown of muscovite +
706 quartz. *Journal of Petrology*, 31, 925–956.
- 707 Brown, M. (2013) Granite: from genesis to emplacement. *Geological Society of American Bulletin*,
708 125, 1079–1113.
- 709 Brown, M., and Rushmer, T., Eds. (2006) *Evolution and Differentiation of the Continental Crust*, 553
710 p. Cambridge University Press, Cambridge.
- 711 Burnham, C.W. (1967) Hydrothermal fluids at the magmatic stage. In: H.L. Barnes, Ed., *Geochemistry*
712 *of Hydrothermal Ore Deposits*, p. 34–76. Holt, Rinehart and Winston, New York. □
- 713 Burnham, C.W. (1975) Water and magmas: a mixing model. *Geochimica et Cosmochimica Acta*, 39,
714 1077–1084.
- 715 Candela, P.A., (1997) A review of shallow, ore-related granites: textures, volatiles and ore metals.

- 716 Journal of Petrology, 38, 1619–1633.
- 717 Carosi, R., Montomoli, C., Langone, A., Turina, A., Cesare, B., Iaccarino, S., Fascioli, L., Visonà, D.,
718 Ronchi, A., and Santa Man, R. (2015) Eocene partial melting recorded in peritectic garnets from
719 kyanite-gneiss, Greater Himalayan Sequence, central Nepal. In: S. Mukherjee, R. Carosi, P. A. van
720 der Beek, B. K. Mukherjee, and D. M. Robinson, Eds., Tectonics of the Himalaya. Geological
721 Society, London, Special Publications 412, pp. 111–129.
- 722 Castro, A., Patiño Douce, A.E., Corretgé, L.G., de la Rosa, J.D., El-Biad, M., and El-Hmidi, H. (1999)
723 Origin of peraluminous granites and granodiorites, Iberian massif, Spain. An experimental test of
724 granite petrogenesis. Contributions to Mineralogy and Petrology, 135, 255–276.
- 725 Cesare, B. (2008) Crustal melting: working with enclaves. In: E.W. Sawyer, and M. Brown, Eds.,
726 Working with Migmatites, p. 37–55. Mineralogical Association of Canada, Short Course 38, Quebec
727 City.
- 728 Cesare, B., and Maineri, C. (1999) Fluid-present anatexis of metapelites at El Joyazo (SE Spain):
729 constraints from Raman spectroscopy of graphite. Contributions to Mineralogy and Petrology, 135,
730 41–52.
- 731 Cesare, B., Salvioli Mariani, E., and Venturelli, G. (1997) Crustal anatexis and melt extraction during
732 deformation in the restitic xenoliths at El Joyazo (SE Spain). Mineralogical Magazine, 61, 15–27.
- 733 Cesare, B., Marchesi, C., Hermann, J., and Gomez-Pugnaire, M.T. (2003a) Primary melt inclusions in
734 andalusite from anatectic graphitic metapelites: Implications for the position of the Al_2SiO_5 triple
735 point. Geology, 31, 573– 576.
- 736 Cesare, B., Meli, S., Nodari, L., and Russo, U., (2005) Fe^{3+} reduction during biotite melting in graphitic
737 metapelites: another origin of CO_2 in granulites. Contributions to Mineralogy and Petrology, 149,
738 129–140.
- 739 Cesare, B., Maineri, C., Baron Toaldo, A., Pedron, D., and Acosta- Vigil, A., (2007) Immiscibility

- 740 between carbonic fluids and granitic melts during crustal anatexis: a fluid and melt inclusion study
741 in the enclaves of the Neogene Volcanic Province of SE Spain. *Chemical Geology*, 237, 433–449.
- 742 Cesare, B., Ferrero, S., Salvioli-Mariani, E., Pedron, D., and Cavallo, A. (2009a) Nanogranite and
743 glassy inclusions: the anatectic melt in migmatites and granulites. *Geology*, 37, 627–630.
- 744 Cesare, B., Acosta-Vigil, A., Ferrero, S., and Bartoli, O. (2011) Melt inclusions in migmatites and
745 granulites. In: M.A. Forster, and J.D. Fitz Gerald, Eds., *The science of microstructure—Part II*,
746 paper 2. *Journal of the Virtual Explorer, Electronic Edition* 38.
- 747 Cesare, B., Acosta-Vigil, A., Bartoli, O., Ferrero, S. (2015) What can we learn from melt inclusions in
748 migmatites and granulites?. *Lithos*, 239, 186–216.
- 749 Chappell, B.W., 1984. Source rocks of I- and S-type granites in the Lachlan Fold Belt, southeastern
750 Australia. *Philosophical Transactions of the Royal Society of London A* 310, 693–707.
- 751 Chappell, B.W. (1999) Aluminium saturation in I- and S-type granites and the characterization of
752 fractionated haplogranites. *Lithos*, 46, 535-551.
- 753 Chappell, B.W., and White, A.J.R. (1974) Two contrasting granite types. *Pacific Geology*, 8, 173–174.
- 754 Chappell, B.W., and White, A.J.R. (1992) I- and S-type granites in the Lachlan Fold Belt. *Transactions*
755 *of the Royal Society of Edinburgh Earth Sciences*, 83, 1–26.
- 756 Chappell, B.W., and White, A.J.R., (2001) Two contrasting granite types: 25 years later. *Australian*
757 *Journal of Earth Sciences*, 48, 489–499.
- 758 Chappell, B.W., White, A.J.R., and Wyborn, D. (1987) The importance of residual source material
759 (restite) in granite petrogenesis. *Journal of Petrology*, 28, 1111–1138.
- 760 Clemens, J.D. (2003) S-type granitic magmas — petrogenetic issues, models and evidence. *Earth*
761 *Science Reviews*, 61, 1–18.
- 762 Clemens, J.D. (2006) Melting of the continental crust: fluid regimes, melting reactions and source-rock
763 fertility. In: M. Brown, and T. Rushmer, Eds., *Evolution and Differentiation of the Continental*

- 764 Crust, p. 297–331. Cambridge University Press, Cambridge.
- 765 Clemens, J.D., and Mawer, C.K. (1992) Granitic magma transport by fracture propagation.
766 Tectonophysics, 204, 339–360.
- 767 Clemens, J.D., and Watkins, J.M. (2001) The fluid regime of high-temperature metamorphism during
768 granitoid magma genesis. Contributions to Mineralogy and Petrology, 140, 600–606.
- 769 Clemens, J.D., and Stevens, G. (2012) What controls chemical variation in granitic magmas?. Lithos,
770 134–135, 317–329.
- 771 Clemens, J.D., and Stevens, G. (2015) Comment on “Water-fluxed melting of the continental crust: A
772 review” by R.F. Weinbert and P. Hasalová. Lithos 234–235, 100–101.
- 773 Clocchiatti, R. (1975) Les inclusions vitreuses des cristaux de quartz. Étude optique, thermooptique et
774 chimique. Applications géologiques, Mémoires de la Société géologique de France, 122, 1–96.
- 775 Conrad, W.K., Nicholls, I.A., and Wall, V.J. (1988) Water-saturated and -undersaturated melting
776 of metaluminous and peraluminous crustal compositions at 10 kbar: Evidence for the origin of
777 silicic magmas in the Taupo volcanic zone, New Zealand, and other occurrences. Journal of
778 Petrology, 29, 765–803.
- 779 Darling, R.S. (2013) Zircon-bearing, crystallized melt inclusions in peritectic garnet from the western
780 Adirondack Mountains, New York State, USA. Geofluids, 13, 453–459.
- 781 DePaolo, D.J. (1981) Trace element and isotopic effects of combined wallrock assimilation and
782 fractional crystallization. Earth and Planetary Science Letters, 53, 189–202.
- 783 Droop, G.T.R., Clemens, J.D., and Dalrymple, J. (2003) Processes and conditions during contact
784 anatexis, melts escape and restite formation: The Huntly Gabbro complex, NE Scotland. Journal of
785 Petrology, 44, 995–1029.
- 786 Ebadi, A., and Johannes, W. (1991) Beginning of melting and composition of first melts in the system
787 Qz–Ab–Or–H₂O–CO₂. Contributions to Mineralogy and Petrology, 106, 286–295.

- 788 Esposito, E., Klebesz, R., Bartoli, O., Klyukin, Y.I., Moncada, D., Doherty, A., and Bodnar, R.J.
789 2012) Application of the Linkam TS1400XY heating stage to melt inclusion studies. *Central*
790 *European Journal of Geosciences*, 4/2, 208–18.
- 791 Farina, F., Albert, C., and Lana C. (2015) The Neoproterozoic transition between medium- and high-K
792 granitoids: Clues from the Southern São Francisco Craton (Brazil). *Precambrian Research*, 266,
793 375–394.
- 794 Faure, F., and Schiano, P. (2005) Experimental investigation of equilibration conditions during
795 forsterite growth and melt inclusion formation. *Earth and Planetary Science Letters*, 236, 882–898.
- 796 Ferrero, S., Bodnar, R.J., Cesare, B., and Viti, C. (2011) Re-equilibration of primary fluid inclusions in
797 peritectic garnet from metapelitic enclaves, El Hoyazo, Spain. *Lithos*, 124, 117–131.
- 798 Ferrero, S., Bartoli, O., Cesare, B., Salvioli-Mariani, E., Acosta-Vigil, A., Cavallo, A., Groppo, C., and
799 Battiston, S. (2012) Microstructures of melt inclusions in anatectic metasedimentary rocks. *Journal*
800 *of Metamorphic Geology*, 30, 303–322.
- 801 Ferrero, S., Braga, R., Berkesi, M., Cesare, B., and Laridhi Ouazaa, N. (2014) Production of
802 metaluminous melt during fluid-present anatexis: an example from the Maghrebian basement, La
803 Galite Archipelago, central Mediterranean. *Journal of Metamorphic Geology*, 32, 209–225.
- 804 Ferrero, S., Wunder, B., Walczak, K., O'Brien, P.J., and Ziemann, M.A. (2015) Preserved near
805 ultrahigh-pressure melt from continental crust subducted to mantle depths. *Geology*, 43, 447–450.
- 806 Ferrero, S., Ziemann, M.A., Angel, R.J., O'Brien, P.J., and Wunder, B. (2016) Kumdykolite,
807 kokchetavite and cristobalite crystallized in nanogranites from felsic granulites, Orlica-Snieznik
808 Dome (Bohemian Massif): not an evidence for ultrahigh pressure conditions. *Contributions to*
809 *Mineralogy and Petrology*, accepted, DOI: 10.1007/s00410-015-1220-x
- 810 Ferri, F., Poli, S., and Vielzeuf, D. (2009) An experimental determination of the effect of bulk
811 composition on phase relationships in metasediments at near-solidus conditions. *Journal of*

- 812 Petrology, 50, 909–93.
- 813 Frezzotti, M.L. (2001) Silicate melt inclusions in magmatic rocks: applications to petrology. *Lithos*, 55,
814 273–99.
- 815 Frost, B.R., and Frost, C.D. (2008) A geochemical classification for feldspathic igneous rocks. *Journal*
816 *of Petrology*, 49, 1955–1969.
- 817 Frost, B.R., Barnes, C.G., Collins, W.J., Arculus, R.J., Ellis, D.J., and Frost, C.D. (2001) A
818 geochemical classification for granitic rocks. *Journal of Petrology*, 42, 2033–2048.
- 819 Gaetani, G.A., O’Leary, J.A., Shimizu, N., Bucholz, C.E., and Newville, M. (2012) Rapid
820 reequilibration of H₂O and oxygen fugacity in olivine-hosted melt inclusions. *Geology*, 40, 915–
821 918.
- 822 García-Casco, A., Haissen, F., Castro, A., El-Hmidi, H., Torres-Roldán, R. L., and Millán, G. (2003)
823 Synthesis of staurolite in melting experiments of a natural metapelite: consequences for phase
824 relations in low-temperature pelitic migmatites. *Journal of Petrology*, 44, 1727–1757.
- 825 Gardien, V., Thompson, A.B., Grujic, D., and Ulmer, P. (1995) Experimental melting of biotite +
826 plagioclase + quartz ± muscovite assemblages and implications for crustal melting. *Journal of*
827 *Geophysical Research*, 100, 15581–15591.
- 828 Gardien, V., Thompson, A.B., and Ulmer, P. (2000) Melting of biotite + plagioclase + quartz gneisses:
829 the role of H₂O in the stability of amphibole. *Journal of Petrology*, 41, 651–666.
- 830 Gualda, G.A., and Ghiorso, M.S. (2013) The Bishop Tuff magma body: an alternative to the Standard
831 Model. *Contributions to Mineralogy and Petrology*, 166, 755–775.
- 832 Gilluly, J., Ed. (1948) *Origin of Granite*, 139 p. Geological Society of America Memoir 28.
- 833 Grant, J.A. (2004) Liquid compositions from low-pressure experimental melting of pelitic rock from
834 Morton Pass, Wyoming, USA. *Journal of Metamorphic Geology*, 22, 65–78.
- 835 Grant, J.A. (2009) THERMOCALC and experimental modeling of melting of pelite, Morton Pass,

- 836 Wyoming. *Journal of Metamorphic Geology*, 27, 571–578.
- 837 Gray, C.M., and Kemp, A.I.S. (2009) The two-component model for the genesis of granitic rocks in
838 southeast- ern Australia—Nature of the metasedimentary-derived and basaltic end members. *Lithos*,
839 111, 113–124
- 840 Groppo, C., Rolfo, F., and Indares, A., (2012) Partial melting in the Higher Himalaya Crystallines of
841 eastern Nepal: the effect of decompression and implications for the “Channel Flow” model. *Journal*
842 *of Petrology*, 53, 1057– 1088.
- 843 Guernina, S., and Sawyer, E.W. (2003) Large-scale melt- depletion in granulite terranes: An example
844 from the Archean Ashuanipi subprovince of Quebec. *Journal of Metamorphic Geology*, 21, 181–
845 201.
- 846 Guillot, S., and Le Fort, P. (1995) Geochemical constraints on the bimodal origin of High Himalayan
847 leucogranites. *Lithos*, 35, 221–234.
- 848 Hacker, R., Kelemen, P.B., and Behn, M.D. (2011) Differentiation of the continental crust by
849 relamination: *Earth and Planetary Science Letters*, 307, 501–516
- 850 Hauri, E. (2002) SIMS analysis of volatiles in silicate glasses, 2: isotopes and abundances in Hawaiian
851 melt inclusions. *Chemical Geology*, 183, 115–141.
- 852 Harris, N., and Massey, J. (1994) Decompression and anatexis of Himalayan metapelites. *Tectonics*,
853 13, 1537–1546.
- 854 Harris, N.B.W., Vance, D., and Ayers, M. (2000) From sediment to granite: Time scales of anatexis in
855 the upper crust. *Chemical Geology*, 162, 155–167
- 856 Hermann, J., and Spandler, C. (2008) Sediment melts at sub-arc depths: an experimental study. *Journal*
857 *of Petrology*, 49, 717–740.
- 858 Holtz, F., and Johannes, W., (1991) Genesis of peraluminous granites: I. Experimental investigation of
859 melt compositions at 3 and 5 kb and various H₂O activities. *Journal of Petrology*, 32, 935–958.

- 860 Holtz, F., Johannes, W., and Pichavant, M. (1992b): Effect of excess aluminium on phase relations in
861 the system Qz-Ab-Or: experimental investigation at 2 kbar and reduced H₂O-activity. *European*
862 *Journal of Mineralogy*, 4, 137–152.
- 863 Huang, W. L., and P. J. Wyllie, (1975) Melting reactions in the system NaAlSi₃O₈-KA1Si₃O₈-SiO₂ to
864 35 kilobars, dry and with excess water *Journal of Geology*, 83, 737–748.
- 865 Huang, W. L. and Wyllie, P. J. (1981) Phase relationships of S-type granite with H₂O to 35 kbar:
866 muscovite granite from Harney Peak, South Dakota. *Journal of Geophysical Research*, 86, 10515–
867 10529.
- 868 Huizenga, J.M., and Touret, J.L.R. (2012) Granulites, CO₂ and graphite. *Gondwana Research* 22, 799–
869 809.
- 870 Iaccarino, S., Montomoli, C., Carosi, R., Massonne, H.-J., Langone, A., Visonà, D. (2015) Pressure–
871 temperature–time–deformation path of kyanite-bearing migmatitic paragneiss in the Kali Gandaki
872 valley (Central Nepal): Investigation of Late Eocene–Early Oligocene melting processes. *Lithos*,
873 231, 103–121.
- 874 Icenhower, J., and London, D., (1995) An experimental study of element partitioning among biotite,
875 muscovite and coexisting peraluminous silicic melt at 200 MPa (H₂O). *American Mineralogist* 80,
876 1229–1251.
- 877 Icenhower, J., and London, D., (1996) Experimental partitioning of Rb, Cs Sr and Ba between alkali
878 feldspar and peraluminous melt. *American Mineralogist*, 81, 719–734.
- 879 Jamieson, R.A., Unsworth, M.J., Harris, N.G.W., Rosenberg, C., and Schulmann, K. (2011) Crustal
880 melting and the flow of mountains. *Elements*, 7, 253–260.
- 881 Johannes, W., and Holtz, F. (1996) *Petrogenesis and experimental petrology of granitic rocks*, 335 p.
882 Berlin, Springer.
- 883 Kawakami, T., Yamaguchi, I., Miyake, A., Shibata, T., Maki, K., Yokoyama, T.D., and Hirata, T.

- 884 (2013) Behavior of zircon in the upper-amphibolite to granulite facies schist/migmatite transition,
885 Ryoke metamorphic belt, SW Japan: constraints from the melt inclusions in zircon. *Contributions to*
886 *Mineralogy and Petrology*, 165, 575–591.
- 887 Kemp, A.I.S., Hawkesworth, C.J., Foster, G.L., Paterson, B.A., Woodhead, J.D., Hergt, J.M., Gray,
888 C.M., and Whitehouse, M.J. (2007) Magmatic and crustal differentiation history of granitic rocks
889 from Hf-O isotopes in zircon. *Science*, 315, 980–983.
- 890 Kent, A.J.R. (2008) Melt inclusions in basaltic and related volcanic rocks. In: K.D. Putirka, and F.J.I.
891 Tepley, Eds., *Minerals, Inclusions and Volcanic Processes*, p. 273–331. *Reviews in Mineralogy and*
892 *Geochemistry*, vol. 69.
- 893 Kesler, S.E., Bodnar, R.J., and Mernagh, T.P. (2013) Role of fluid and melt inclusion studies in
894 geologic research. *Geofluids*, 13, 398–404.
- 895 Koester, E., Pawley, A.R., Fernandes, L.A.D., Porcher, C.C., and Soliani Jr., E. (2002) Experimental
896 melting of cordierite gneiss and the petrogenesis of syntranscurrent peraluminous granites in
897 southern Brazil. *Journal of Petrology*, 43, 1595–1616.
- 898 Korhonen, F.J., Saito, S., Brown, M., Siddoway, C.S. (2010) Modeling multiple melt loss events in the
899 evolution of an active continental margin. *Lithos*, 116, 230–248.
- 900 Kretz, R. (1983) Symbols for rock-forming minerals. *American Mineralogist*, 68, 277–279.
- 901 Le Breton, N., and Thompson, A.B. (1988) Fluid-absent (dehydration) melting of biotite in metapelites
902 in the early stages of crustal anatexis. *Contributions to Mineralogy and Petrology*, 99, 226–237.
- 903 Le Fort, P. (198). Manaslu leucogranite: a collision signature of the Himalaya. A model for its genesis
904 and emplacement. *Journal of Geophysical Research*, 86, 10545–10568.
- 905 Le Fort, P., Cuney, M., Deniel, C., France-Lanord, C., Sheppard, S. M. F., Upreti, B. N., and Vidal, P.
906 (1987) Crustal generation of the Himalayan leucogranites. *Tectonophysics*, 134, 39–57.
- 907 Leshner, C.E., Walker, D., Candela, P., and Hays, J.F. (1982) Soret fractionation of natural silicate melts

- 908 of intermediate to silicic composition. Geological Society of America Abstracts with Programs 14,
909 545.
- 910 Litvinovsky, B.A., Steele, I.M., and Wickham, S.M. (2000) Silicic magma formation in overthickened
911 crust: Melting of charnockite and leucogranite at 15, 20 and 25 kbar. *Journal of Petrology*, 41, 717–
912 737.
- 913 López, S., Castro, A., García-Casco, A. (2005) Production of granodiorite melt by interaction between
914 hydrous mafic magma and tonalitic crust. Experimental constraints and implications for the
915 generation of Archaean TTG complexes. *Lithos*, 79, 229–250.
- 916 Luth, W.C., Jahns, R.H., and Tuttle, O.F. (1964) The granite system at pressure of 4 to 10 kilobars.
917 *Journal of Geophysical Research*, 69, 759–773.
- 918 Maheshwari, A., Coltorti, M., Sial, A.N., and Mariano, G., (1996) Crustal influences in the
919 petrogenesis of the Malani rhyolite, southwestern Rajasthan: Combined trace element and oxygen
920 isotope constraints. *Journal of the Geological Society of India*, 47, 611–619.
- 921 Massare, D., Metrichm, N., and Clocchiatti, R. (2002) High-temperature experiments on silicate melt
922 inclusions in olivine at 1 atm: inference on temperatures of homogenization and H₂O concentrations.
923 *Chemical Geology* 183, 87–98.
- 924 Massonne, H.J. (2014) Wealth of P–T–t information in medium-high grade metapelites: Example from
925 the Jubrique Unit of the Betic Cordillera, S Spain. *Lithos* 208–209, 137–157.
- 926 Miller, C. F., McDowell, S. M., and Mapes, R. W. (2003) Hot and cold granites? Implications of zircon
927 saturation temperatures and preservation of inheritance. *Geology*, 31, 529–532.
- 928 Milord, I., Sawyer, E.W., and Brown, M. (2001) Formation of diatexite migmatite and granite magma
929 during anatexis of semipelitic metasedimentary rocks: An example from St. Malo, France. *Journal*
930 *of Petrology*, 42, 487–505.
- 931 Montel, J.M., and Vielzeuf, D. (1997) Partial melting of metagreywackes. Part II. Compositions of

- 932 minerals and melts. *Contributions to Mineralogy and Petrology*, 128, 176–196.
- 933 Morgan, G.B.VI, and London, D. (1996) Optimizing the electron microprobe analysis of hydrous alkali
934 aluminosilicate glasses. *American Mineralogist*, 81, 1176–1185. □
- 935 Morgan G.B.VI, and London, D. (2005a) Effect of current density on the electron microprobe analysis
936 of alkali aluminosilicate glasses. *American Mineralogist*, 90, 1131–1138.
- 937 Morgan G.B.VI, and London, D. (2005b) Phosphorus distribution between potassic alkali feldspar □ and
938 metaluminous haplogranitic liquid at 200 MPa (H₂O): the effect of undercooling on crystal–liquid
939 systematics. *Contributions to Mineralogy and Petrology*, 150, 456–471.
- 940 Mosca, P., Groppo, C., and Rolfo, F. (2012) Structural and metamorphic features of the Main Central
941 Trust Zone and its contiguous domains in the eastern Nepalese Himalaya. *Journal of Virtual
942 Explorer*, paper 2, Electronic Edition 41.
- 943 Nair, R., and Chacko, T. (2002) Fluid-absent melting of high-grade semi-pelites: P–T constraints on
944 orthopyroxene formation and implications for granulite genesis. *Journal of Petrology*, 43, 2121–
945 2141.
- 946 O' Connor, J.T. (1965) A classification for quartz-rich igneous rocks based on feldspar ratios. U.S.
947 Geological Survey Professionnal Paper 525, 79–84.
- 948 Olsen, S.N., and Grant, J.A. (1991) Isocon analysis of migmatization in the Front Range, Colorado
949 USA. *Journal of Metamorphic Geology*, 9, 151–164.
- 950 Pandit, M.K., Shekhawat, L.S., Ferreira, V.P., Sial, A.N., and Bohra, S.K. (1999) Trondhjemite and
951 granodiorite assemblages from west of Barmer: probable basement for malani Magmatism in
952 western India. *Journal Geological Society of India*, 53, 89–96.
- 953 Patiño Douce, A. E., and Beard, J. S. (1995) Dehydration-melting of biotite gneiss and quartz
954 amphibolite from 3 to 15 kbar. *Journal of Petrology*, 36, 707–738.
- 955 Patiño Douce, A. E., and Beard, J. S. (1996) Effects of P, f (O₂) and Mg/ Fe ratio on dehydration-

- 956 melting of model metagreywackes. *Journal of Petrology*, 37, 999–1024.
- 957 Patiño Douce, A.E., and Johnston, A.D. (1991) Phase equilibria and melt productivity in the pelitic
958 system: implications for the origin of peraluminous granitoids and aluminous granulites.
959 *Contributions to Mineralogy and Petrology* 107, 202–218.
- 960 Patiño Douce, A.E., and Harris, N. (1998) Experimental constraints on Himalayan anatexis. *Journal of*
961 *Petrology*, 39, 689–710.
- 962 Peto, P. (1976) An experimental investigation of melting relationships involving muscovite and
963 paragonite in the silica-saturated portion of the system $K_2O-Na_2O-Al_2O_3-SiO_2-H_2O$ to 15 kbar total
964 pressure. In: *Progress in Experimental Petrology*, 3rd Report, p. 41–45 London: NERC.
- 965 Pickering, J.M., and Johnston, D.A., (1998) Fluid-absent melting behaviour of a two mica metapelite:
966 experimental constraints on the origin of Black Hill Granite. *Journal of Petrology*, 39, 1787–1804.
- 967 Portnyagin, M., Almeev, R., Matveev, S., and Holtz, F. (2008) Experimental evidence for rapid H_2O
968 exchange between melt inclusions in olivine and host magma. *Earth and Planetary Science Letters*,
969 272, 541–552.
- 970 Read, H.H. (1948) Granites and granites. In: J. Gilluly, Ed., *Origin of Granite*, p. 1–19. Geological
971 Society of America Memoir 28.
- 972 Roedder, E. (1979) Origin and significance of magmatic inclusions. *Bulletin of Mineralogy*, 102, 487–
973 510.
- 974 Roedder, E. (1984) *Fluid Inclusions*, Reviews in Mineralogy, vol. 12. Washington, DC: Mineralogical
975 Society of America.
- 976 Rosenberg, C.L., and Handy, M.R. (2005) Experimental deformation of partially melted granite
977 revisited: implications for the continental crust. *Journal of Metamorphic Geology*, 23, 19–28.
- 978 Sawyer, E.W. (2008) *Atlas of Migmatites*. Mineralogical Association of Canada, The Canadian
979 Mineralogist Special Publication 9, Quebec City.

- 980 Sawyer, E.W., Cesare, B., and Brown, M. (2011) When the continental crust melts. *Elements*, 7 , 229–
981 234.
- 982 Santosh, M., and Omori, S. (2008) CO₂ flushing: a plate tectonic perspective. *Gondwana Research*, 13,
983 86–102.
- 984 Scaillet B., France-Lanord, C., and Le Fort P. (1990) Badrinath-Gangotri plutons (Garhwal, India):
985 petrological and geochemical evidence for fractionation processes in a high Himalayan leucogranite.
986 *Journal of Volcanology and Geothermal Research*, 44, 163–188.
- 987 Scaillet, B., Pichavant, M., and Roux, J. (1995) Experimental crystallization of leucogranite magmas.
988 *Journal of Petrology*, 36, 664–706.
- 989 Schiano, P. (2003) Primitive mantle magmas recorded as silicate melt inclusions in igneous minerals.
990 *Earth Science Reviews*, 63, 121–144.
- 991 Schmidt, M.W., Vielzeuf, D., and Auzanneau, E. (2004) Melting and dissolution of subducting crust at
992 high pressures: the key role of white mica. *Earth and Planetary Science Letters* 228, 65–84.
- 993 Sharma, K.K. (2004) The Neoproterozoic Malani magmatism of the northwestern India shield:
994 implications for crust-building processes. *Proceedings Indian Academy of Science*, 113, 795–807.
- 995 Singh J., and Johannes, W. (1996) Dehydration melting of tonalities. Part II. Composition of melts and
996 solids. *Contributions to Mineralogy and Petrology*, 125, 26–44.
- 997 Skjerlie, K.P., and Johnston, A.D. (1993) Fluid-absent melting behavior of an F-rich tonalitic gneiss at
998 med-crustal pressures: implications for the generation of anorogenic granites. *Journal of Petrology*,
999 34, 785–815.
- 1000 Slagstad, T., Jamieson, R.A., and Culshaw, N.G. (2005) Formation, crystallization, and migration of
1001 melt in the mid-orogenic crust: Muskoka domain migmatites, Grenville Province, Ontario. *Journal*
1002 *of Petrology*, 46, 893–919.
- 1003 Sobolev, A.V. (1996) Melt inclusions in minerals as a source of principle petrological information.

- 1004 Petrology, 4, 209–220.
- 1005 Solar, G.S., and Brown, M. (2001) Petrogenesis of migmatites in Maine, USA: Possible source of
1006 peraluminous leucogranite in plutons: *Journal of Petrology*, 42, 789–823
- 1007 Sorby, H.C. (1858) On the microscopical structure of crystals, indicating origin of minerals and rocks.
1008 *Quarterly Journal of the Geological Society of London* 14, 453–500.
- 1009 Spicer, E.M., Stevens, G., and Buick, I.S. (2004) The low-pressure partial-melting behaviour of natural
1010 boron-bearing metapelites from the Mt. Stafford area, central Australia. *Contributions to Mineralogy
1011 and Petrology*, 148, 160–179.
- 1012 Symmes, G.H., and Ferry, J.M. (1995) Metamorphism, fluid-flow and partial melting in pelitic rocks
1013 from the Onawa contact aureole, central Maine, USA: *Journal of Petrology*, 36, 587–612.
- 1014 Stevens, G., Villaros, A., and Moyen, J.-F. (2007) Selective peritectic garnet entrainment as the origin
1015 of geochemical diversity in S-type granites. *Geology* 35, 9–12.
- 1016 Sun, S. S. and McDonough, W. F. (1989) Chemical and isotopic systematics of oceanic basalts:
1017 implications for mantle composition and processes. In: A.D. Saunders and M.J. Norry, Eds.,
1018 *Magmatism in the Ocean Basins*, p. 313–345. Geological Society, London, Special Publications 42.
- 1019 Thomas, R., and Davidson, P. (2012) H₂O in granite and pegmatite-forming melts. *Ore Geology
1020 Reviews*, 46, 32–46.
- 1021 Thompson, A.B. (1990) Heat, Fluids, and Melting in the Granulite Facies. In: D., Vielzeuf, D. and Ph.
1022 Vidal, Eds., *Granulites and Crustal Evolution*, p. 37–57. NATO ASI Series Volume 311.
- 1023 Tropper, P., Konzett, J., and Finger, F. (2005) Experimental constraints on the formation of high-P/high
1024 T granulites in the Southern Bohemian Massif. *European Journal of Mineralogy*, 17, 343–356.
- 1025 Tuttle, O.F., and Bowen, N.L. (1958) Origin of granite in the light of experimental studies in the
1026 system: NaAlSi₃O₈–KAlSi₃O₈–SiO₂–H₂O. *Geological Society of America Memoir* 74, 153 p.
- 1027 Vernon, R.H. (2010) Granites really are magmatic: using microstructural evidence to refute some

- 1028 obstinate hypotheses. In: M.A. Forster, and J.D. Fitz Gerald, Eds., The science of microstructure—
1029 Part I, paper 1. Journal of the Virtual Explorer, Electronic Edition 35.
- 1030 Vielzeuf, D., and Holloway, J.R. (1988) Experimental determination of the fluid-absent melting
1031 relations in the pelitic system. Contributions to Mineralogy and Petrology, 98, 257–76.
- 1032 Villaros, A., Stevens, G., Moyen, J.F., and Buick, I.S. (2009). The trace element compositions of S-
1033 type granites: evidence for disequilibrium melting and accessory phase entrainment in the source.
1034 Contributions to Mineralogy and Petrology, 158, 543–561.
- 1035 Visonà, D., Carosi, R., Montomoli, C., Peruzzo, L., and Tiepolo, M. (2012) Miocene andalusite
1036 leucogranite in central-east Himalaya (Everest–Masang Kang area): low-pressure melting during
1037 heating. Lithos, 144, 194–208.
- 1038 Wall, V.J., Clemens, J.D., and Clarke, D.B. (1987) Models for granitoid evolution and source
1039 compositions. Journal of Geology, 95, 731–750.
- 1040 Ward, R., Stevens, G., and Kisters, A. (2008) Fluid and deformation induced partial melting and melt
1041 volumes in low-temperature granulite-facies metasediments, Damara Belt, Namibia. Lithos, 105,
1042 253–271.
- 1043 Webb, G., Powell, R., and McLaren, S. (2015) Phase equilibria constraints on the melt fertility of
1044 crustal rocks: the effect of subsolidus water loss. Journal of Metamorphic Geology, 33, 147–165.
- 1045 Weinberg, R.F., and Hasalová, P. (2015a) Water-fluxed melting of the continental crust: A review.
1046 Lithos, 212-215, 158–188.
- 1047 Weinberg, R.F., and Hasalová, P. (2015b) Reply to comment by J.D. Clemens and G. Stevens on
1048 'Water-fluxed melting of the continental crust: A review'. Lithos, 234-235, 102–103.
- 1049 Weinberg, R.F., Sial, A.N., and Pessoa, R.R. (2001) Magma flow within the Tavares pluton,
1050 northeastern Brazil: compositional and thermal convection. Geological Society of America Bulletin
1051 113, 508–520.

1052 Wilke S., Klahn C., Bolte T., Almeev R., and Holtz F. (2015) Experimental investigation of the effect
1053 of Ca, Fe and Ti on cotectic compositions of the rhyolitic system. *European Journal of Mineralogy*,
1054 DOI: 10.1127/ejm/2015/0027-2423

1055 White, R.W., Stevens, G., and Johnson, T.E. (2011) Is the crucible reproducible? Reconciling melting
1056 experiments with thermodynamic calculations. *Elements*, 7, 241–246.

1057 Yakymchuk, C., Brown, C.B., Brown, M., Siddoway, C., Fanning, C.M., and Korhonen, F.J. (2015)
1058 Paleozoic evolution of western Marie Byrd Land, Antarctica. *Geological Society of American*
1059 *Bulletin*, 127, 1464–1484.

1060 Zeck, H.P. (1970) An erupted migmatite from Cerro de Hoyazo, SE Spain. *Contributions to*
1061 *Mineralogy and Petrology*, 26, 225–246.

1062

1063 **Figure captions**

1064 **FIGURE 1.** Schematic T-t diagram showing the main processes occurring during melt production
1065 (heating or prograde path) and melt consumption (cooling or retrograde path) in the partially melted
1066 continental crust. MI can be trapped during incongruent melting (arrow 1) and igneous crystallization
1067 (arrow 5). Mineral abbreviations after Kretz (1983). Ideal incongruent melting reaction from Vielzeuf
1068 and Holloway (1988).

1069

1070 **FIGURE 2.** Photomicrographs of primary nanogranitoid inclusions. **(a)** Garnet porphyroblasts from a
1071 partially melted pelitic enclave from El Hoyazo, SE Spain (additional information in Cesare et al.,
1072 1997). MI are distributed in zonal arrangements (red arrows). **(b)** Peritectic garnet in porphyroblastic
1073 gneisses from the anatectic sequence of Jubrique, Betic Cordillera, S Spain (see also Barich et al.,
1074 2014). Square: area enlarged in (c). **(c)** Close-up of inner part of the garnet crystal in (b) where clusters
1075 of micrometric inclusions are present. The presence of MI clusters with random distribution

1076 unequivocally demonstrates their primary nature. **(d, e)** Plane-polarized and crossed polars images
1077 respectively of the crystallized inclusion marked by a red arrow in (c). Multiple birefringent phases are
1078 recognizable within the inclusion.

1079

1080 **FIGURE 3.** SEM backscattered images **(a-e)** and plane-polarized light photomicrograph **(f)** of the
1081 microstructures of melt inclusions. **(a)** Fully crystallized nanogranite in khondalites (India). **(b)** Fully
1082 crystallized MI from Bohemian Massif. In this case, polymorphs have been identified by Raman
1083 spectroscopy (Ferrero et al., 2016). **(c)** Partially crystallized inclusion with internal porosity (red
1084 arrows, respectively) from Ronda metatexites. **(d)** Glassy MI in anatectic enclaves from the Neogene
1085 Volcanic Province, SE Spain. **(e)** Coexistence of glassy and crystallized MI in Ronda diatexites. **(f)**
1086 Cluster of associated fluid and melt inclusions (red and yellow arrows), indicative of fluid
1087 immiscibility in a graphite-bearing crustal enclaves.

1088

1089 **FIGURE 4.** Harker diagrams showing the major element concentrations (wt%) of melt inclusions in
1090 crustal enclaves and in migmatites and granulites (data from Supplementary Tables 1¹ and 2¹ of
1091 Supporting Information). **(a)** SiO₂ vs. Al₂O₃. **(b)** SiO₂ vs. Na₂O. **(c)** SiO₂ vs. K₂O. **(d)** SiO₂ vs.
1092 FeO_T+MgO+TiO₂. **(e)** SiO₂ vs. CaO. Numbers in parentheses indicate the number of analyses for each
1093 case study.

1094

1095 **FIGURE 5.** Chondrite-normalized trace element patterns (normalizing values from Sun and
1096 McDonough, 1989). **(a)** Normalized trace element patterns for melt inclusions in crustal enclaves of
1097 NVP, SE Spain (from Acosta-Vigil et al., 2010). **(b)** Normalized trace element patterns for melt
1098 inclusions in migmatites from Ojen, S Spain (Bartoli, unpublished data). The average upper continental
1099 crust composition is reported for comparison (data from Rudnick and Gao, 2014).

1100

1101 **FIGURE 6.** An-Or-Ab diagram with fields for granite, quartz-monzonite, granodiorite, trandhjemite and
1102 tonalite after O'Connor (1965). Symbols as in Figure 4.

1103

1104 **FIGURE 7.** Plot of ASI [aluminum saturation index = molar $\text{Al}_2\text{O}_3/(\text{CaO}+\text{Na}_2\text{O}+\text{K}_2\text{O})$] vs. AI [alkalinity
1105 index = molar $\text{Al}_2\text{O}_3-(\text{Na}_2\text{O}+\text{K}_2\text{O})$; see Frost and Frost, 2008]. Dotted line separates the compositional
1106 fields of I- and S-type granites s.l. (from Chappell and White, 1974; Chappell, 1999). Symbols as in
1107 Figure 4.

1108

1109 **FIGURE 8.** Geochemical classification of crustal melts following Frost et al. (2001) and Frost and Frost
1110 (2008). (a) Fe-index [$\text{FeO}_T/(\text{FeO}_T+\text{MgO})$] vs. SiO_2 (wt%). (b) MALI (modified alkali-lime index =
1111 $\text{Na}_2\text{O} + \text{K}_2\text{O} - \text{CaO}$) vs. SiO_2 (wt%). Data on a volatile free basis. Symbols as in Figure 4.

1112

1113 **FIGURE 9.** (a) CIPW Qtz-Ab-Or diagram showing the normative compositions of all analyzed
1114 nanogranitoid melt inclusions. Symbols as in Figure 4. Black dots and lines show the eutectic points
1115 and cotectic lines for the subaluminous haplogranite system at $a_{\text{H}_2\text{O}} = 1$ and different pressures (Holtz
1116 et al., 1992; Luth et al., 1964; Huang and Wyllie, 1975). References to experimental glasses: PDJ91,
1117 950 °C, 7 kbar (Patiño Douce and Johnston, 1991); D03, 900 °C, 5 kbar (Droop et al., 2003); GC03,
1118 675-775 °C, 6-14 kbar, H_2O -present (Garcia-Casco et al., 2003); PDH98, 700-775 °C, 6-10 kbar, H_2O -
1119 present (Patiño Douce and Harris, 1998); SF15: 870-950 °C, 16-30 kbar (see Ferrero et al., 2015). (b)
1120 Normative Qtz-Ab-Or diagram showing the displacement of eutectic points and cotectic lines as a
1121 function of P, $a_{\text{H}_2\text{O}}$, An and Al_2O_3 contents. Black dots and lines as in (a). Light blue arrow: effect of
1122 increasing pressure (Johannes and Holtz, 1996 and references therein). Red arrows: effect of decreasing

1123 $a_{\text{H}_2\text{O}}$ at 2, 5 and 10 kbar (white dots are eutectic points at different $a_{\text{H}_2\text{O}}$; Ebadi and Johannes, 1991;
1124 Becker et al., 1998). Violet arrow: effect of increasing Al content at 2 kbar and $a_{\text{H}_2\text{O}}=0.5$, i.e. from a
1125 subaluminous to peraluminous system (Holtz et al., 1992). Green arrow: effect of increasing An
1126 content at 2 kbar and $a_{\text{H}_2\text{O}}=0.5$. With the addition of An the phase diagram changes to a eutectic system
1127 with respect to the haplogranite system with a minimum (see green lines; Wilke et al., 2015). Double
1128 grey arrow: effect of diffusive transport properties of the melt on the composition of experimental
1129 glasses (Acosta-Vigil et al., 2006). It should be noted that the addition of significant amounts of B and
1130 F to the system (>1 wt%) moves eutectic points and cotectic lines towards Ab-rich compositions
1131 (Johannes and Holtz, 1996). However, the effects of B and F are not reported here because these
1132 elements are present in very low amounts in the investigated MI (< 0.1 wt%; Acosta-Vigil et al., 2007).
1133 See text for details.

1134
1135 **FIGURE 10. (a)** Variation diagram showing the trace element contents for glassy MI and matrix glass in
1136 the crustal enclaves hosted in El Hoyazo dacite (NVP, SE Spain). **(b)** Zircon and monazite saturation
1137 temperatures calculated for all analyzed glasses of enclaves. Symbols as in (a). Diagonal line marks the
1138 geometrical location of points where both temperatures coincide. **(c)** Prograde history of melt formation
1139 in the continental crust beneath the Neogene Volcanic Province of SE Spain, estimated by accessory
1140 mineral saturation temperatures (redrawn after Acosta-Vigil et al., 2010). The relevant experimentally-
1141 determined melting reactions in the granitic and metapelitic systems are reported. HW81 refers to
1142 Huang and Wyllie (1981), P76 to Peto (1976), PDH98 to Patiño Douce and Harris (1998), PDJ91 to
1143 Patiño Douce and Johnston (1991) and VH88 to Vielzeuf and Holloway (1988).

1144
1145 **FIGURE 11.** Compositions (in mol%) of analyzed nanogranitoid melt inclusions in terms of

1146 (Fe_{Tot}+Mg+Ti), (Na+Ca), (Si+Al)/10 and K (after Solar and Brown, 2001; Barnes et al., 2002). The
1147 compositional fields of major crystalline phases and host rocks are reported. Bulk compositions of
1148 crystalline rocks are from Bartoli (2012), Groppo et al. (2012), Ferrero et al. (2014, 2015) and
1149 Iaccarino et al. (2015). Data for KKB rocks are not available. In the case of El Hoyazo samples, both
1150 chemical compositions of i) Grt-Bt and Crd-Sp enclaves and ii) low-grade metapelites from the
1151 Alpujarride basement (considered to approximate the source composition before melt extraction) are
1152 plotted (data from Cesare et al., 1997). **(a, b)** (Fe_{Tot}+Mg+Ti)–(Na+Ca)–K diagrams for MI from
1153 crystalline rocks (a) and from crustal enclaves (b). **(c, d)** (Fe_{Tot}+Mg+Ti)–(Na+Ca)–(Si+Al)/10 diagrams
1154 for MI from crystalline rocks (c) and from crustal enclaves (d). **(e, f)** Comparison between MI and
1155 crustal magmas. Manaslu leucogranites: data from Le Fort (1981, 1987) and Guillot and Le Fort
1156 (1995). Gangotri leucogranites: data from Scaillet et al. (1990). Everest/Masang Kang leucogranites:
1157 data from Visonà et al. (2012). Layos granite: data from Barbero and Villaseca (1992). Manali
1158 rhyolites: data from Maheshwari et al. (1996) and Sharma (2004). Yellow stars containing black dots
1159 indicate metaluminous or peralkaline Malani rhyolites. See text for details.

1160
1161 **FIGURE 12.** Comparison among the Fe_{Tot}+Mg+Ti, (Na+Ca), (Si+Al)/10 and K concentrations (in
1162 mol%) of melt inclusions and glasses from partial melting experiments. Experimental glasses were
1163 produced at T=650-950 °C, P=1-50 kbar, variable a_{H2O} and from metasedimentary and felsic (SiO₂≥62
1164 wt%) (meta)granitoid protoliths. Data from: Conrad et al. (1988); Le Breton and Thompson (1988);
1165 Vielzeuf and Holloway (1988); Brearley and Rubie (1990); Patiño Douce and Johnston (1991); Holtz
1166 and Johannes (1991); Skjerlie and Johnston (1993); Icenhower and London (1995, 1996); Gardien et al.
1167 (1995, 2000); Patiño Douce and Beard (1995, 1996); Singh and Johannes (1996); Montel and Vielzeuf
1168 (1997); Patiño Douce and Harris (1998); Pickering and Johnston (1998); Castro et al. (1999);
1169 Litvinovsky et al. (2000); Koester et al. (2002); Nair and Chacko (2002); García-Casco et al. (2003);

1170 Droop et al. (2003); Grant (2004, 2009); Schmidt et al. (2004); Spicer et al. (2004); Lopez et al. (2005);
1171 Tropper et al. (2005); Acosta-Vigil et al. (2006); Auzanneau et al. (2006); Watkins et al. (2007);
1172 Hermann and Spandler (2008); Ward et al. (2008); Ferri et al. (2009). Compositions of melt inclusions
1173 and major crystalline phases as in Fig. 11. Red dots: experimental glasses produced at 700°C and 5-15
1174 kbar (from Koester et al., 2002). Dashed black lines reflect the maximum $Fe_{Tot}+Mg+Ti$ contents
1175 reported for low-temperature (650-720 °C) experimental glasses, with the exception of analyses
1176 reported in Koester et al. (2002). See text for details.

1177

1178

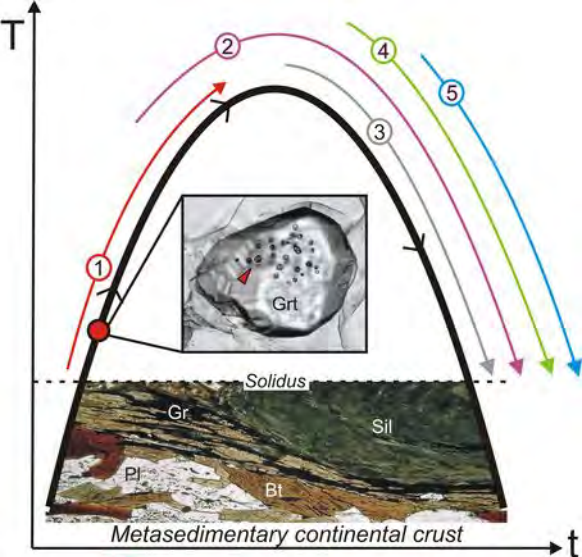
1179

1180 **TABLE 1.** Occurrences of nanogranitoid melt inclusions discussed in the text.

Locality	Host rocks	Host minerals	T, P conditions	Reference
Neogene Volcanic Province (NVP), SE Spain	Metapelitic enclave	Grt, Pl, And, Crd, Ilm	≈615-850, ≈2-7 kbar	1, 2, 3, 4, 5, 6
Ojén, Ronda, S Spain	Quartzo-feldspathic metatexite	Grt	≈660-700, ≈4.5-5 kbar	7, 8
Ojén, Ronda, S Spain	Quartzo-feldspathic diatexite	Grt	≈820, ≈6-6.5 kbar	9
La Galite, Tunisia	Tonalitic and garnetitic enclave	Grt	≈770-820, ≈5 kbar	10
Barun, Nepal Himalaya	Gneiss	Grt	≈800-860, ≈8 kbar	11
Kerala Khondalite Belt (KKB), S India	Khondalites	Grt	≈900, ≈6-8 kbar	11, 12
Orlica-Śnieżnik Dome, Bohemian Massif	Felsic granulite	Grt	≈875, ≈27 kbar	13

1181

1182 1: Acosta-Vigil et al. (2007); 2: Acosta-Vigil et al. (2010); 3: Acosta-Vigil et al. (2012); 4: Cesare et al. (2003); 5: Cesare et al. (2007);
 1183 6: Ferrero et al. (2011); 7: Bartoli et al. (2013a); 8: Bartoli et al. (2013b); 9: Bartoli et al. (2015); 10: Ferrero et al. (2014); 11: Ferrero et
 1184 al. (2012); 12 Cesare et al. (2009); 13: Ferrero et al. (2015).



① Melt formation and MI entrapment
 $Bt + Sil + Pl + Qtz = Grt + \text{melt} (\pm Kfs)$

② Melt segregation

③ Magma crystallization and differentiation

④ Volatile degassing

⑤ Entrapment of "classic" MI

